Article:

Olumayegun, O., Wang, M. and Kelsall, G. (2017) Thermodynamic analysis and preliminary design of closed Brayton cycle using nitrogen as working fluid and coupled to small modular Sodium-cooled fast reactor (SM-SFR). Applied Energy, 191. pp. 436-453. ISSN 0306-2619

https://doi.org/10.1016/j.apenergy.2017.01.099

Thermodynamic Analysis and Preliminary Design of Closed Brayton Cycle Using Nitrogen as Working Fluid and Coupled to Small Modular Sodium-cooled Fast Reactor (SM-SFR)

Olumide Olumayegun[a], Meihong Wang[a], Greg Kelsall[b]

[a] Process and Energy Systems Engineering Group, School of Engineering, University of Hull, Cottingham Road, Hull, HU6 7RX, United Kingdom

[b] GE Power, Newbold Road, Rugby, CV21 2NH, Warwickshire, United Kingdom

Abstract

Sodium-cooled fast reactor (SFR) is considered the most promising of the Generation IV reactors for their near-term demonstration of power generation. Small modular SFRs (SM-SFRs) have less investment risk, can be deployed more quickly, are easier to operate and are more flexible in comparison to large nuclear reactor. Currently, SFRs use the proven Rankine steam cycle as the power conversion system. However, a key challenge is to prevent dangerous sodium-water reaction that could happen in SFR coupled to steam cycle. Nitrogen gas is inert and does not react with sodium. Hence, intercooled closed Brayton cycle (CBC) using nitrogen as working fluid and with a single shaft configuration has been one common power conversion system option for possible near-term demonstration of SFR. In this work, a new two shaft nitrogen CBC with parallel turbines was proposed to further simplify the design of the turbomachinery and reduce turbomachinery size without compromising the cycle efficiency. Furthermore, thermodynamic performance analysis and preliminary design of components were carried out in comparison with a reference single shaft nitrogen cycle. Mathematical models in Matlab were developed for steady state thermodynamic analysis of the cycles and for preliminary design of the heat exchangers, turbines and compressors. Studies were performed to investigate the impact of the recuperator minimum terminal temperature difference (TTD) on the overall cycle efficiency and recuperator size. The effect of turbomachinery efficiencies on the overall cycle efficiency was examined. The results showed that the cycle efficiency of the proposed configuration was comparable to the 39.44% efficiency of the reference cycle. In addition, the study indicated that the new configuration has the potential to simplify the design of turbomachinery, reduce the size of turbomachinery and provide opportunity for improving the efficiency of the turbomachinery. The findings so far revealed that the proposed two-shaft CBC with nitrogen as working fluid could be a promising power conversion system for SM-SFRs near-term demonstration.

Keywords

Sodium-cooled fast reactor

Closed Brayton cycle

Nitrogen working fluid

Thermodynamic analysis

Heat exchanger design

Turbomachinery design

Highlights

- Nitrogen closed Brayton cycle for small modular sodium-cooled fast reactor studied
- Thermodynamic modelling and analysis of closed Brayton cycle performed
- Two-shaft configuration proposed and performance compared to single shaft
- Preliminary design of heat exchangers and turbomachinery carried out

Nomenclature and Units

Abbreviations

2-D	Two-dimensional
ASTRID	Advanced Sodium Technological Reactor for Industrial Demonstration
CBC	closed Brayton cycle
CDT	compressor-driving turbine
FPT	free power turbine
Gen IV	Generation IV
GIF	Gen IV International Forum
HPC	high pressure compressor
IHX	intermediate heat exchanger
LMTD	logarithmic mean temperature difference
LPC	low pressure compressor
Na/N_2 IHX	sodium/nitrogen intermediate heat exchanger
NIST	National Institute of Standards and Technology
PCHE	Printed Circuit Heat Exchanger
PCS	power conversion system
s-CO_2	supercritical carbon dioxide
SFR	sodium-cooled fast reactor
SM-SFR	small modular sodium-cooled fast reactor
SMR	small modular reactor
TTD	terminal temperature difference

Symbols

A	Area (m^2)
AR	Aspect ratio
b_H	Blade height (m)
c	Blade chord (m)
C	Absolute velocity (m/s)
C_L	Lift coefficient
Cp	Specific heat capacity at constant pressure
D	Diameter (m)
DF	Diffusion factor
$dHaller$	de Haller number
d_s	Specific diameter
f	Darcy friction factor
g	Gravitational acceleration (m/s^2)

H	Head (m)
h	Specific enthalpy (kJ/kg) or convective heat transfer coefficient [W/(m^2.K)]
k	Thermal conductivity [W/(m.K)]
L	Length (m)
ln	Natural logarithm
$\dot{m}$	Mass flow rate (kg/s)
min	Minimum
n_s	Specific speed
N_b	Number of blade
Nu	Nusselt number
op	Optimum value
P	Pressure (Pa or N/m^2)
Pr	Prandtl Number
$\dot{Q}$	Volumetric flow rate (m^3/s)
Q	Heat duty (watt or J/s)
r	Radius (m)
Re	Reynold number
s	Blade spacing (m)
T	Temperature (K)
t	Conduction length (m)
U	Overall heat transfer coefficient [W/(m^2.K)] or blade velocity (m/s)
V	Velocity (m/s)
W	Power (W or J/s) or relative velocity (m/s)
α	Absolute velocity angle (degree)
β	Relative velocity angle (degree)
Δ	Change in quantity
δ	Fluid deflection through blade
ε	Effectiveness or pipe roughness
η	Efficiency
Λ	Reaction
μ	Viscosity (Pa-s)
ξ	Relative pressure loss or blade nominal loss coefficient
π	Pressure ratio or pi
ρ	Density (kg/m^3)
σ	Blade solidity
ϕ	Flow coefficient
ψ	Stage loading coefficient
ω	Rotational speed (rev/s)

Subscripts

0	Stagnation property
1	Turbine or compressor stage inlet
2	Turbine rotor or compressor stator inlet
3	Turbine or compressor stage exit
ad	adiabatic
C	Compressor
c	Cold stream
$elec$	Electrical
ex	Exit
gen	Generator

h	Hot stream or hydraulic
HX	Heat exchanger
i	inlet
is	Isentropic
N_2	Nitrogen
Na	Sodium
m	Melting or mean-line
max	Maximum
o	Outlet
P	Pump
RX	Reactor
T	Turbine or Temperature
tt	Total-to-total
x	Axial component
θ	Tangential component

1 Introduction

Generation IV nuclear reactors (Gen IV reactors) are the next step in the deployment of nuclear power generation to meet the world's future energy demand [1]. Of all the six Gen IV reactors, sodium-cooled fast reactor (SFR) has been identified as the most matured and hence the most suitable for near-term demonstration [2-4]. In addition to the larger SFRs, Small Modular Sodium-cooled Fast Reactors (SM-SFRs) with plant size ranging from 50 to 300 MWe are also under consideration by Gen IV International Forum (GIF) [5]. Generally, small modular reactors (SMRs) are viewed to have less financial risk, cheaper when mass produced, could be deployed faster, and are easier to operate and maintain compared with larger nuclear reactor [6, 7]. Most of the components could be factory-built and then assemble on site. In addition, SMRs are more flexible with respect to their generation and location due to their lower capacity. Therefore, SMRs could help cope with the challenge of intermittent renewable energy by rapidly increasing or decreasing power output [8-11]. Also, it can be sited in off-grid areas requiring small power and future growth can be accommodated by simply adding extra units.

The power conversion system (PCS) implementation is critical to the successful commercialization of the SM-SFR power plant technology. The current SFRs (e.g. Phenix, SuperPhenix, BN 600, BN 800, e.t.c.) adopt the proven Rankine steam cycle as PCS [12, 13]. However, there are concerns over the coupling of steam cycle to SFR. The challenges include: (1) safety concern because of the possibility of hazardous sodium-water reaction (2) high capital cost because of additional secondary sodium circuit and large plant footprint, and (3) low efficiency. Therefore, closed Brayton cycle (CBC) is considered as a promising alternative PCS for SFRs. Recently, Olumayegun et al carried out a review of the research activities and studies performed worldwide on CBC [14]. Use of CBC has the potential to simplify the design, reduce technical risk, reduce the amount and size of equipment and improve efficiency. Working fluids consider for the CBC include supercritical CO_2 (s-CO_2), helium and nitrogen.

In 1966, Feher patented the supercritical cycle heat engine and the possibility of using s-CO_2 cycle for nuclear power generation was later investigated [14, 15]. Recent times has witnessed a renewed interest in s-CO_2 cycle [16] as PCS for nuclear power [17-19] and other heat sources such as concentrated solar power [20-22], fuel cell [23], coal [24] and waste heat[25]. In literature, s-CO_2 cycle has been investigated as alternative to steam cycle for SFR application [3, 26-32]. All the studies agreed on the benefits of s-CO_2 CBC power conversion system for SFR including higher efficiency (about 44%) and smaller footprint. However, sodium-CO_2 reaction could be of safety concern at some temperatures and requires further investigation to understand the nature of the chemical reaction [29, 33]. Also, s-CO_2 CBC still requires major technological developments for the turbomachinery and heat exchangers [3, 29]. Helium gas does not react with sodium but helium CBC is not promising for SFRs due to its low thermal efficiency [12]. The nitrogen CBC option is attractive because nitrogen is inert, thus eliminating the risk of sodium-water or sodium-CO_2 reactions. Furthermore, design of nitrogen PCS is anticipated to be less challenging since years of experience from air gas turbine engines can be applied [34]. After all, nitrogen properties are similar to those of air. Hence, the nitrogen cycle was perceived as the only potential option for short-term demonstration while the s-CO_2 cycle could be a suitable option for long-term applications [12, 35].

The nitrogen gas Brayton cycle is mainly been developed in France under the ASTRID (Advanced Sodium Technological Reactor for Industrial Demonstration) SFR project [35-37] . Cachon et al. [37] presented different feasibility studies and heat exchanger design for innovative power conversion systems for ASTRID SFR. The result led to the selection of nitrogen gas Brayton cycle. Alpy et al. [35] performed a comparison in terms of the thermodynamic performance and preliminary components sizing between nitrogen and s-CO_2 cycle for the ASTRID SFR. The s-CO_2 cycle has a higher efficiency (about 44%) than the nitrogen cycle (about 38%). However, the nitrogen cycle was chosen for near-term demonstration of electricity generation from CBC coupled to SFR. Ahn and Lee investigated several CBC designs for SM-SFR as alternatives to the Rankine steam cycle [7]. CBC using s-CO_2, helium and nitrogen as working fluids was compared in term of thermodynamic performance and physical size of the components. Recently, Seo et al. [13] investigated the adoption of nitrogen power conversion system for a SM-SFR. Nitrogen working fluid was chosen ahead of s-CO_2 and helium considering both safety and thermal performance as well as the elimination of intermediate sodium loop. Sensitivity studies were performed to optimise the system and the effect of the elimination of intermediate (secondary) sodium loop on the thermodynamic efficiency of the plant was studied. The study showed that the elimination of the intermediate loop increased the thermodynamic efficiency by 3% point.

The aim of this paper is the thermodynamic analysis and preliminary design of components of CBC using nitrogen as working fluid and coupled to SM-SFR for near-term demonstration of electricity generation from Gen IV reactors. The often suggested configuration for the nitrogen cycle is the intercooled CBC with single shaft, in which all the compressors, turbine and generator rotates at the grid frequency. However, preliminary design of the turbomachinery indicated that the design of the turbine is especially difficult [38]. One solution for simplifying and improving the design of turbomachinery is to change the shaft rotational speed. This requires the use of either frequency converter or gearbox, both of which will incur efficiency penalty. Moreover, maximum practical power output for which a gearbox is feasible is about 80 MW [39]. Another option is to employ a two-shaft configuration in which the generator and a free power turbine (FPT) rotate at the grid frequency while the compressors and a compressor-driving turbine (CDT) rotate at an independent shaft speed. The free selection of a higher compressors shaft speed can then be used to optimise the design of the compressors and the driving turbine. This will result in reduced stage numbers and more compact turbomachinery as well as possible improvement of turbomachinery efficiency. Two layouts are possible for the two-shaft configuration. One is to have the FPT and the CDT in series and the other is to have them in parallel. The two-shaft with parallel turbines layout is adopted in this study as the series turbines layout is known to result in loss of overall cycle efficiency [40].

To the best of our knowledge, no one has investigated a two-shaft configuration option for nitrogen cycle coupled to SFR. Also, most previous studies of CBC tend to be limited to thermodynamic performance analysis [3, 6, 13]. In summary, the main novel contributions of this article are: (a) a new two-shaft nitrogen CBC with parallel turbines was proposed as a way to further simplify the design of the turbomachinery and reduce turbomachinery size without compromising the cycle efficiency (b) thermodynamic performance analysis were carried out in comparison with a reference single shaft nitrogen cycle (c) preliminary design of components were performed for the proposed and the reference configurations. Further effort in this work to estimate the sizes of components through preliminary design can be crucial to the economic assessment of the plants. The effect of the recuperator minimum terminal temperature difference (TTD) on the cycle efficiency and recuperator size was investigated. The impact of changes in turbomachinery efficiency on the overall cycle efficiency was examined. The thermodynamic performances and preliminary designs were evaluated using the Matlab codes developed for cycle analysis, heat exchanger design, axial compressor design and axial turbine design. The performance calculation and preliminary design were performed for nitrogen Brayton cycles coupled to a SFR with thermal power of 500 MW and reactor exit temperature of 545 °C.

The structure of the paper is as follows. Section 2 describes the layout of the reference single-shaft and the proposed two-shaft with parallel turbines configuration. Section 3 outlines the methodology for cycle thermodynamic modelling and performance analysis. In Section 4 the methodology for the preliminary design of the heat exchangers and turbomachinery is presented. Section 5 presents the results and discussion of the thermodynamic analysis and preliminary design for the nitrogen cycles. Finally, conclusions are drawn in Section 7.

2 Plant configurations and description

In this study, two nitrogen CBC configurations have been considered: a reference single-shaft intercooled closed-cycle gas turbine configuration and a two-shaft with parallel turbines configuration. The single-shaft intercooled configuration seems to be the most popular design choice for nitrogen CBC. Hence it will be used as reference case for comparison with the suggested alternative two-shaft configuration. A more detailed description of the two configurations will be presented in this section.

2.1 Reference single-shaft intercooled closed Brayton cycle

The schematic flow diagram of the reference single-shaft intercooled CBC is shown in Figure 1. In this configuration, all the turbomachinery rotates on a single shaft. The plant features a 500 MWth SFR coupled indirectly to the PCS through the sodium/nitrogen intermediate heat exchanger (Na/N_2 IHX). The primary circuit is made up of the SFR reactor, the primary side of Na/N_2 IHX and the sodium pump. Sodium coolant at 545 °C and 1.15 bar exits the reactor core and flows through the primary side of the IHX. The pump is used to circulate the liquid sodium in the primary circuit. Thus the reactor core heat is transferred to the PCS via the Na/N_2 IHX. The PCS is connected to the secondary side of the Na/N_2 IHX and uses nitrogen as working fluid. The Brayton cycle consists of two compressors referred to as low pressure compressor (LPC) and high pressure compressor (HPC), a turbine and four heat exchangers (Na/N_2 IHX, recuperator, precooler and intercooler).

The temperature-entropy (T-S) diagram of the closed Brayton PCS is illustrated in Figure 2. High temperature nitrogen leaving the Na/N_2 IHX at 530 °C is expanded in the turbine to produce mechanical power. The power produced by the turbine is used to drive the electrical generator, the LPC and the HPC connected to the same shaft. The shaft rotates at the grid synchronous speed of 3000 rpm since the generator is directly connected to the grid. Part of the residual heat energy in the low pressure nitrogen exiting the turbine is recovered in the recuperator. The nitrogen gas then enters the precooler where the remaining heat energy is rejected to the surrounding through the cooling water. The cooled nitrogen at 27 °C is compressed in the LPC, cooled again in the intercooler to 27 °C and compressed to the maximum cycle pressure of 180 bar by the HPC. It then enters the high pressure side of the recuperator where it is preheated with the heat energy recovered from the fluid leaving the turbine. After recuperation, the fluid passes through the secondary side of the Na/N_2 IHX. At the outlet of the Na/N_2 IHX the nitrogen gas achieves the highest temperature within the cycle after absorbing heat from liquid sodium flowing through the primary side. The hot nitrogen gas is then routed to the turbine to repeat the thermodynamic cycle.

2.2 Two-shaft with parallel turbines closed Brayton cycle

The schematic diagram of the proposed alternative two-shaft configuration is shown in Figure 3. It is similar to the reference case except that (a) it uses two parallel turbines referred to as compressor-driving turbine (CDT) and free power turbine (FPT), and (b) it employs two independent rotor shafts referred to as compressor shaft and generator shaft. The CDT drives the LPC and the HPC through the compressor shaft while the FPT drives the electrical generator through the generator shaft. The main nitrogen flow exiting the Na/N_2 IHX is split into two streams at the turbines inlet. The first stream is expanded in the CDT rotating at speed higher than 3000rpm. The flow through this turbine is just enough to drive the LPC and the HPC. The second stream flow through the FPT rotating at 3000 rpm to match the grid frequency and generate electric power.

A significant feature of the two-shaft parallel turbines configuration is that the compressor shaft speed can be selected to minimise the technical design challenges of the turbomachines as their design could be optimised for non-grid rotational speed. Also the use of two parallel turbines instead of series arrangement helps to maintain the thermal efficiency of the PCS [40] as well as reduce the volumetric flow through the turbines.

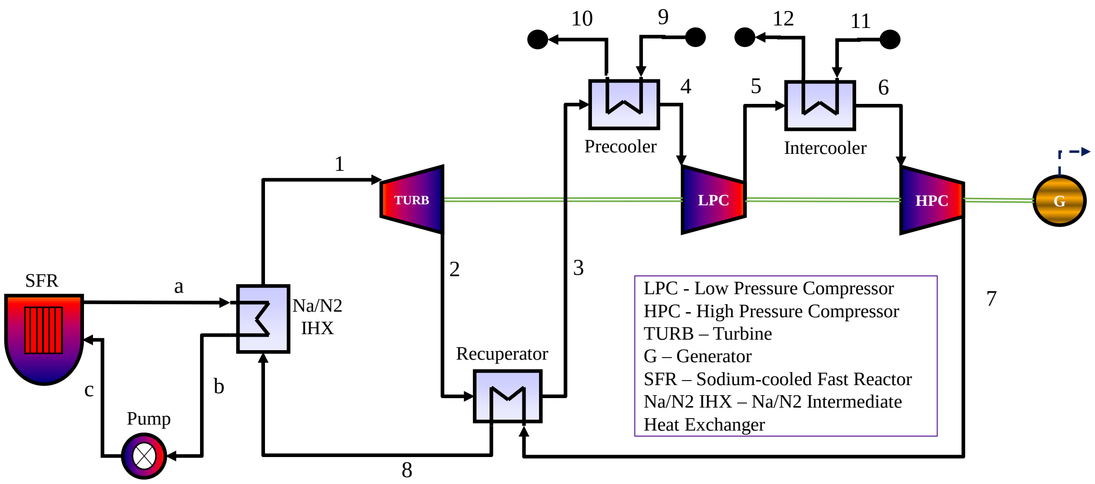

Figure 1 Reference single-shaft closed Brayton cycle [7, 35]

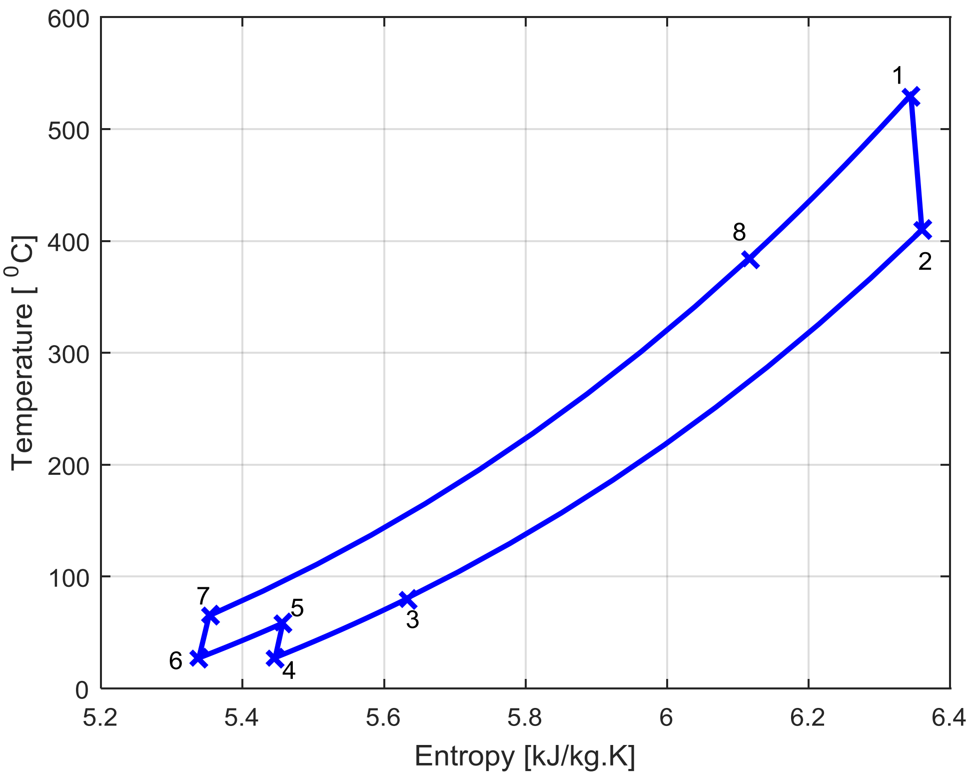

Figure 2 Temperature-Entropy diagram

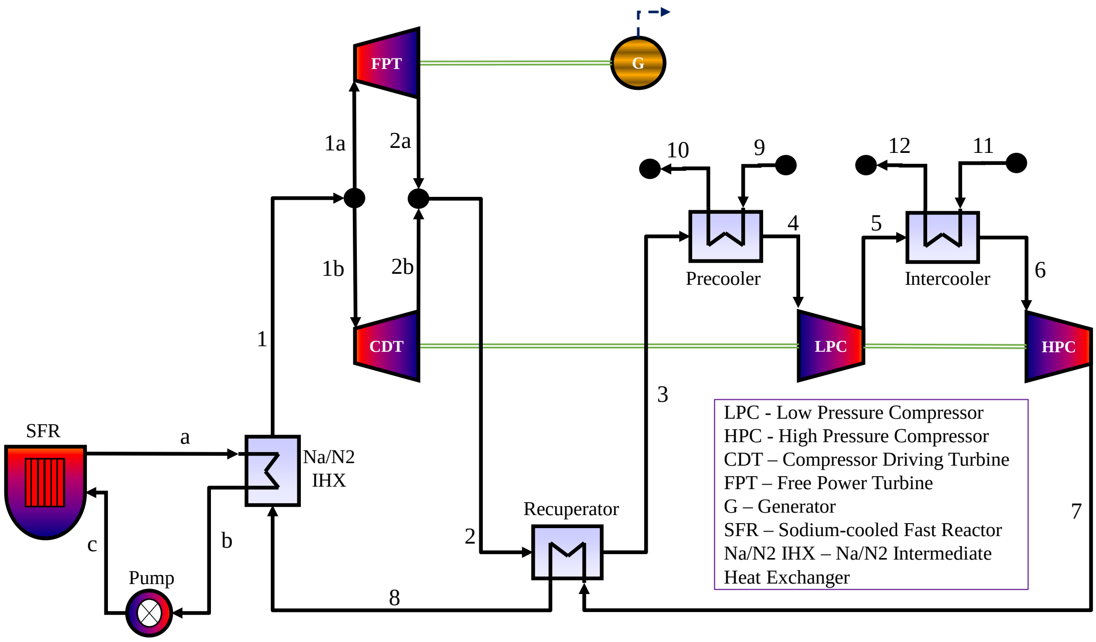

Figure 3 Proposed two-shaft closed Brayton cycle with turbines in parallel

3 Thermodynamic analysis and cycle modelling

3.1 Thermodynamic modelling of cycle components and performance evaluation

Using Matlab, a cycle analysis code was developed for CBC coupled to SFR. Steady state thermodynamic performance of the nitrogen CBC was evaluated with the Matlab code. The cycle calculation code consists of models of the SFR reactor, pump, IHX, recuperator, precooler, intercooler, compressors, turbines and pipes. Models of the individual component were derived based on steady state mass and energy balances, thermodynamic relations and characteristic equations of the components.

Assumed known were: reactor thermal power; core outlet temperature and pressure; cycle maximum pressure; hot side outlet temperatures of intermediate heat exchanger (IHX), precooler and intercooler; turbomachinery isentropic efficiencies; minimum TTD or effectiveness of heat exchangers; generator efficiency; and relative pressure losses of pipes and heat exchangers. Consequently, the mass flows, fluid thermodynamic states, heat transferred, mechanical power delivered or absorbed, generator output and cycle efficiency were evaluated. The whole cycle calculation process begins with initial guesses for the LPC and HPC pressure ratios. The iteration is continued until optimum values of compressor ratios in term of the maximum cycle efficiency are obtained. Note that any thermodynamic property can be obtained from the fluid thermodynamic property sources if two independent properties are known.

The reactor was modelled as a heat source. For the given reactor thermal power, the primary circuit sodium mass flow rate was calculated using equation (1)

$$Q_{RX} = \dot{m}_{Na}(h_{RXo} - h_{RXi}) \tag{1}$$

Where,

Q_{RX} is reactor thermal power
$\dot{m}_{Na}$ is the mass flow rate of sodium coolant
h_{RXo} is the specific enthalpy of sodium at reactor outlet
h_{RXi} is the specific enthalpy of sodium at reactor inlet

The liquid sodium is recycled by the pump. The external power input in the pump is given as:

$$W_P = \dot{m}_{Na}(h_{Po} - h_{Pi}) \tag{2}$$

Where,

W_P is pump power
h_{Po} is the specific enthalpy at pump outlet
h_{Pi} is the specific enthalpy at pump inlet

The pump isentropic efficiency is:

$$\eta_{P,is} = \frac{h_{Po,is} - h_{Pi}}{h_{Po} - h_{Pi}} \tag{3}$$

Where,

$\eta_{P,is}$ is the pump isentropic efficiency
$h_{Po,is}$ is the ideal specific enthalpy at pump outlet with isentropic pressure rise

For an isentropic process in the pump, it follows that the first law for closed system undergoing reversible process becomes:

$$h_{Po,is} - h_{Pi} = \frac{P_{Po} - P_{Pi}}{\rho_{Pi}} \quad (4)$$

Where,

P_{Po} is the pump outlet pressure

P_{Pi} is the pump inlet pressure

ρ_{Pi} is the density of sodium at pump inlet

The compressors were modelled using their pressure ratios and isentropic efficiencies. The compressor outlet conditions were computed from equation (5) and (6):

$$P_{Co} = P_{Ci}\pi \quad (5)$$

Where,

P_{Co} is the compressor outlet pressure

P_{Ci} is the compressor inlet pressure

π is the pressure ratio

$$\eta_{C,is} = \frac{h_{Co,is} - h_{Ci}}{h_{Co} - h_{Ci}} \quad (6)$$

Where,

$\eta_{C,is}$ is the isentropic efficiency of the compressor

$h_{Co,is}$ is the ideal specific enthalpy at compressor outlet with isentropic compression

h_{Ci} is the specific enthalpy at compressor inlet

h_{Co} is the specific enthalpy at compressor outlet

The power consumption of the compressors, W_C is calculated as the product of nitrogen mass flow, $\dot{m}_{N2}$ and enthalpy rise between the inlet and outlet of the compressors.

$$W_C = \dot{m}_{N2}(h_{Co} - h_{Ci}) \quad (7)$$

Similarly, the turbines were modelled using the pressure ratios and isentropic efficiencies. The pressure, enthalpy and power were calculated by using equation (8), (9) and (10).

$$P_{To} = \frac{P_{Ti}}{\pi} \quad (8)$$

Where,

P_{To} is the turbine outlet pressure

P_{Ti} is the turbine inlet pressure

$$\eta_{T,is} = \frac{h_{Ti} - h_{To}}{h_{Ti} - h_{To,is}} \quad (9)$$

Where,

$\eta_{T,is}$ is the isentropic efficiency of the turbine

$h_{To,is}$ is the ideal specific enthalpy at turbine outlet with isentropic expansion

h_{Ti} is the specific enthalpy at turbine inlet

h_{To} is the specific enthalpy at turbine outlet

$$W_T = \dot{m}_{N2}(h_{Ti} - h_{To}) \quad (10)$$

Where W_T is the power delivered by the turbine

The IHX, recuperator, precooler and intercooler were modelled as counter flow heat exchangers. Two calculation options are available. The first option is to assume that the minimum TTD is known while the second option is to assume that the effectiveness is known. Using the TTD approach, the minimum TTD can occur either at the hot end (hot stream inlet/cold stream outlet) or at the cold end (cold stream inlet/hot stream outlet). As an initial guess, the TTD was assumed to occur at the hot end, then:

$$T_{co} = T_{hi} - TTD \tag{11}$$

Where,

T_{co} is the cold stream outlet temperature
T_{hi} is the hot stream inlet temperature

Therefore, the heat exchanger duty (heat transferred), Q_{HX} is:

$$Q_{HX} = \dot{m}_c(h_{co} - h_{ci}) \tag{12}$$

Where,

$\dot{m}_c$ is the cold stream mass flow rate
h_{co} is the cold stream outlet specific enthalpy
h_{ci} is the cold stream inlet specific enthalpy

Then the hot stream outlet enthalpy is:

$$h_{ho} = h_{hi} - \frac{Q_{HX}}{\dot{m}_h} \tag{13}$$

Where,

$\dot{m}_h$ is the hot stream mass flow rate
h_{ho} is the hot stream outlet specific enthalpy
h_{hi} is the hot stream inlet specific enthalpy

If the temperature difference at cold end is discovered to be lower than the TTD, equation (11) is replaced with equation (14). Then the above calculation is repeated but starting with cold end.

$$T_{ho} = T_{ci} + TTD \tag{14}$$

Where,

T_{ho} is the hot stream outlet temperature
T_{ci} is the cold stream inlet temperature

However, if the effectiveness approach is to be used, the exchanger effectiveness, ε_{HX} is defined as:

$$\varepsilon_{HX} = \frac{\dot{m}_c(h_{co} - h_{ci})}{Q_{max}} = \frac{\dot{m}_h(h_{hi} - h_{ho})}{Q_{max}} \tag{15}$$

The maximum theoretical heat transfer rate in counter flow heat exchanger of infinite heat transfer surface area, Q_{max}, is given as follows:

$$Q_{max} = min\{(\dot{m}_c(h_{co_{Thi}} - h_{ci})); (\dot{m}_h(h_{hi} - h_{hoTci}))\} \tag{16}$$

Where,

$h_{co_{Thi}}$ is the outlet enthalpy of cold stream at the temperature of the hot stream inlet
h_{hoTci} is the outlet enthalpy of the hot stream at the cold stream inlet temperature

Inlet or outlet pressures of heat exchangers and pipes were calculated from the relative pressure losses defined as:

$$\xi = \frac{P_i - P_o}{P_i} \tag{17}$$

Where,

P_i is the inlet pressure

P_o is the outlet pressure

The cycle thermodynamic states of pressure, temperature and enthalpy at all component inlet and outlet were obtained by solving the equations (1) - (17). Then the electrical power supplied to the grid, W_{elec} was calculated as:

$$W_{elec} = \eta_{gen}\left(\sum W_T - \sum W_C\right) - W_P \tag{18}$$

Where η_{gen} is the electrical generator efficiency

Note that pump power was not considered negligible in the cycle calculation. This will reduce the plant efficiency. The cycle efficiency, η_{cycle} is defined as the ratio of electrical power output to the reactor thermal power:

$$\eta_{cycle} = \frac{W_{elec}}{Q_{RX}} \tag{19}$$

The cycle analysis code is further integrated with the heat exchanger preliminary design code/program. Heat exchanger design was performed based on the mass flows and fluid conditions determined through the cycle calculation, and a chosen maximum pressure loss constraint. Then the initial heat exchanger pressure losses used for cycle calculation is replaced with the actual pressure losses obtained from the preliminary design code. The process is repeated iteratively until there is convergence of the mass flows and fluid conditions. On the other hand, the turbomachininery design code determined the number of stages and size of the turbines and compressors.

3.2 Fluid thermodynamic and transport properties

The liquid sodium in the primary circuit carries the heat energy to be transferred to the PCS, nitrogen gas is the working fluid in the PCS while liquid water in the cold side of the precooler and intercooler is used for heat rejection to the environment. Hence the cycle analysis and the preliminary design codes must be able to simulate the fluid properties of liquid sodium, nitrogen gas and liquid water. Fluid thermodynamic properties to be simulated include: pressure, temperature, enthalpy, density, heat capacity and speed of sound. Transport properties include the dynamic viscosity and thermal conductivity.

Since Matlab does not have any thermodynamic and transport property function, a Matlab code was written to compute the properties of liquid sodium. The computations were based on correlations recommended by Sobolev [41]. A summary of the correlations used to generate property values of liquid sodium is given in Table 1. The effect of pressure on the thermodynamic and transport properties of liquid sodium was neglected. However, properties of nitrogen and liquid water were obtained from REFPROP (version 9.1) program of the National Institute of Standards and Technology (NIST). The REFPROP program has been reported to be accurate and widely applicable to a variety of pure fluid and mixtures [42, 43]. Any unknown properties can be requested from the REFPROP program by supplying two known independent properties. Both the Matlab code for liquid sodium property and the REFPROP program were used as subroutines in the cycle analysis and preliminary design codes.

Table 1
Correlations for computing liquid sodium properties

Property	**Correlations (T is in Kelvins)**	**Units**
Enthalpy	$h = 164.8(T - T_m) - 1.97 \times 10^{-2}(T^2 - T^2{}_m) + 4.167 \times 10^{-4}(T^3 - T^3{}_m) + 4.56 \times 10^5(T^{-1} - T^{-1}{}_m);\ T_m = melting\ temperature$	J/kg
Density	$\rho = 1014 - 0.235T$	kg/m^3
Specific heat capacity	$Cp = -3.001 \times 10^6 T^{-2} + 1658 - 0.8479T + 4.454 \times 10^{-4} T^2$	J/kgK
Viscosity	$\ln\mu = \frac{556.835}{T} - 0.3958 \ln T - 6.4406$	$Pa - s$
Thermal conductivity	$k = 110 - 0.0648T + 1.16 \times 10^{-5} T^2$	W/mK

3.3 Model validation

The model for the nitrogen CBC was verified with results of numerical model reported by Ahn and Lee [7]. The input parameters used for the validation are shown in Table 2. In Table 3, the main results of the cycle model are compared with the literature values. The results of the cycle model agreed well with the results obtained from literature to within 0.86%. The small dissimilarities in the results could be due to the thermodynamic properties calculations and the round-off error in the input parameters. Therefore, the developed Matlab cycle model is deemed accurate enough for simulating the performance of the nitrogen CBC.

Table 2
Input parameters for the validation of the nitrogen CBC. Data taken from Ahn and Lee [7]

Parameters	Value
Cycle maximum pressure	181.5 bar
LPC/HPC inlet temperature	27 ^{0}C
Turbine inlet temperature	500 ^{0}C
IHX Na side inlet temperature	526 ^{0}C
IHX Na side outlet temperature	450 ^{0}C
Recuperator minimum TTD	14.2 ^{0}C
Turbine efficiency	90%
LPC/HPC efficiency	85%
Thermal work	150 MW

Table 3
Validation of cycle model against literature value

Parameters	Literature value [7]	Simulation value	Relative difference (%)
Precooler inlet temperature	90.7 ^{0}C	90.6 ^{0}C	0.11
LPC outlet temperature	59.4 ^{0}C	59.4 ^{0}C	0
HPC outlet temperature	76.5 ^{0}C	76.5 ^{0}C	0
IHX N2 side inlet temperature	348.7 ^{0}C	348.6 ^{0}C	0.03
Turbine outlet temperature	373.3 ^{0}C	373.4 ^{0}C	0.03
Recuperator effectiveness	95%	95.1%	0.11
Nitrogen mass flow	2510.0 kg/s	2508.9 kg/s	0.04
Thermal efficiency	34.9%	35.2%	0.86

3.4 Assumptions and settings

Some boundary conditions and parameters have to be set in order to evaluate the thermodynamic performance of the cycles. In this study, the selection of the boundary conditions and parameters were done within the limits allowed by the state-of-the-art in component technologies (e.g. turbine and compressor) and values obtained in open literatures [3, 7, 35, 44].

Therefore, the following assumptions and settings were used for the thermodynamic performance calculation:

- Steady state full power rating conditions were assumed
- Negligible heat losses to the surrounding except through the cooling water in precooler and intercooler
- The heat source was assumed to be a SM-SFR with a constant reactor thermal input of 500 MW
- A reactor core outlet temperature of 545 °C and pressure of 1.15 bar were selected while IHX Na side outlet temperature was set to 395 °C
- Since pipe design is outside the scope of this study, the pressure losses along the pipes were set to zero
- Pressure loss through the reactor core was set at 3.74 bar
- Turbomachinery were assumed to be adiabatic with isentropic efficiencies of 93%, 89%, 88% and 82% for the turbines, LP compressors, HP compressors and pump respectively
- LPC and HPC inlet temperatures were set at 27 °C
- Heat exchangers were designed as Printed Circuit Heat Exchanger (PCHE) type.
- Heat exchanger models were based on the TTD (or pinch) approach. Specifying heat exchanger performance in term of minimum TTD or pinch, instead of effectiveness, is considered to be a more realistic measure of what is achievable [45]
- Turbine inlet temperature was set to 530 °C. This has been selected higher than the values reported in most literature since this study eliminates the use of intermediate sodium loop
- Recuperator minimum TTD was set to 15 °C
- Precooler and intercooler cooling water inlet temperatures were assumed to be available at 20 °C. Hence the precooler and intercooler TTD was about 7 °C
- Generator efficiency was taken to be 98.7%
- Maximum cycle pressure at HPC outlet was set at 180 bar

- The compressors inlet pressures were defined by the optimum pressure ratios, which were determined by optimisation to the cycle efficiency

These assumed baseline conditions and parameters only represent a realistic starting point for cycle performance calculation and comparison. Hence for sensitivity analysis, some of these values could be varied to examine their effects on the cycle performance and component design.

4 Preliminary design of heat exchangers and turbomachinery

The main components having significant impact on the performance and size of CBC are the heat exchangers and turbomachinery. Therefore, this section describes the methodology for their preliminary design and sizing. Design of the primary circuit components such as the reactor and sodium pump was not considered. Also piping design was not examined.

4.1 Heat exchanger design and sizing methodology

Preliminary design and sizing was done for the following heat exchangers: Na/N_2 IHX, recuperator, precooler and intercooler. Appropriate selection and design of heat exchangers for CBC is important because [46]: (1) The volume of the heat exchangers will largely determine the footprint of the CBC and hence the capital cost (2) The effectiveness and pressure losses through the heat exchangers will impact the cycle efficiency and hence the operating cost (3) Reliable heat exchangers that is able to withstand the CBC's high pressure and temperature will guarantee the safety of the plant.

All the heat exchangers in this work were assumed to be of the PCHE type. Most previous studies settled on the PCHE as the heat exchanger of choice for CBC [17, 44, 47] . This is due to its compactness, reliable mechanical characteristics at high pressure and temperature and the high effectiveness [48]. Heatric Ltd (UK) has been the sole manufacturer of PCHE since 1985. PCHEs are constructed from flat metal plates into which fluid flow channels are photo-chemically etched into one side of the plate. The etched-out plates are then stacked and diffusion bonded together to form strong, compact, all-metal heat exchanger module as shown in Figure 4. The etched channels are usually semi-circular in cross-section with typical diameter of 1.0 – 5.0 mm and depth of 0.5 – 2.5 mm [49]. According to Heatric, it is possible to manufacture PCHE module with size up to 900 mm (width) by 900 mm (height) by 2500 mm (length) if desired [35]. The calculations in this work were based on the standard plate and flow channel specifications shown in Table 4. The hot and cold plate specifications were assumed to be the same. Straight flow channels with counter-current flow arrangement was also assumed in the design. Depending on the required thermal duty, a number of identical modules are then welded together to form the complete heat exchanger unit [50].

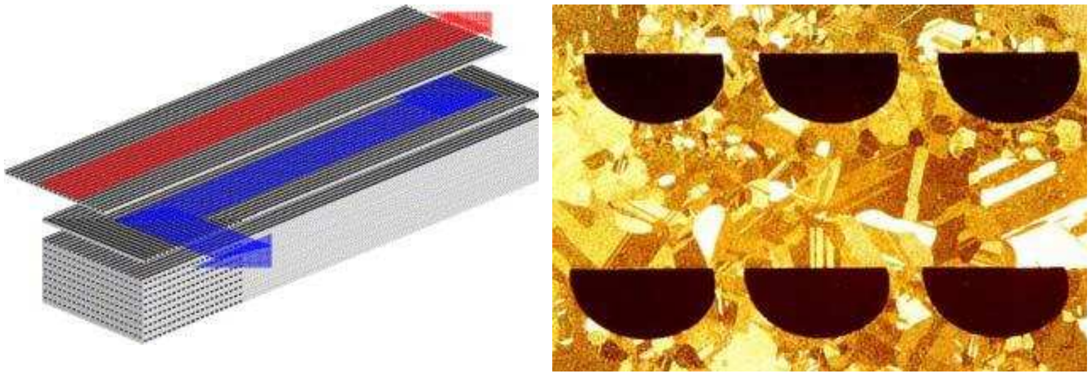

a. PCHE plate stacking

b. Micrograph section through diffusion bonded core

Figure 4 Printed circuit heat exchanger construction (courtesy of Heatric)

Table 4
Selected PCHE specifications

Specification	**Value**
Material	316L Stainless steel
Channel diameter	1.5-2 mm
Channel pitch	1.9 - 2.4 mm
Plate thickness	1-1.5 mm
Module width	900 mm
Module height	about 900 mm
Module length	<= 2500 mm

A preliminary heat exchanger design code, which can be integrated with the cycle calculation code, was developed in Matlab. The cycle calculation provided some of the initial design conditions such as the fluid types, mass flow rates, inlet and outlet enthalpies, inlet pressures and effectiveness. The heat exchanger design code then uses the given initial design conditions, the PCHE plate specifications and the desired maximum pressure drop to estimates the size and mass of the heat exchanger. The code calculates the flow frontal cross section area (width X height) and the length of the heat exchanger that meet the required effectiveness while satisfying the maximum pressure loss requirement. The design was carried out based on the logarithmic mean temperature difference (LMTD) method. For proper determination of fluid properties within the heat exchanger, the flow paths along the heat exchanger is discretised into N number of thermal nodes as shown in Figure 5. The specific heat of the fluid can be assumed to be constant within the thermal nodes such that the LMTD can be calculated as follows:

$$LMTD = \frac{(T_{ho} - T_{ci}) - (T_{hi} - T_{co})}{\ln \dfrac{(T_{ho} - T_{ci})}{(T_{hi} - T_{co})}} \tag{20}$$

The heat transferred is given by:

$$Q = \dot{m}_c(h_{co} - h_{ci}) = \dot{m}_h(h_{hi} - h_{ho}) = U.A.LMTD \tag{21}$$

The overall heat transfer coefficient, U was determined from the convective heat transfer coefficients and conduction through the heat exchanger material as follows:

$$\frac{1}{U} = \frac{1}{h_h} + \frac{t}{k} + \frac{1}{h_c} \tag{22}$$

Where,

h_h is the convective heat transfer coefficient on the hot side

h_c is the convective heat transfer coefficient on the cold side

Convective heat transfer coefficients were determined based on the Nusselt number formula:

$$Nu = \frac{hD_h}{k} \tag{23}$$

Where D_h is the hydraulic diameter

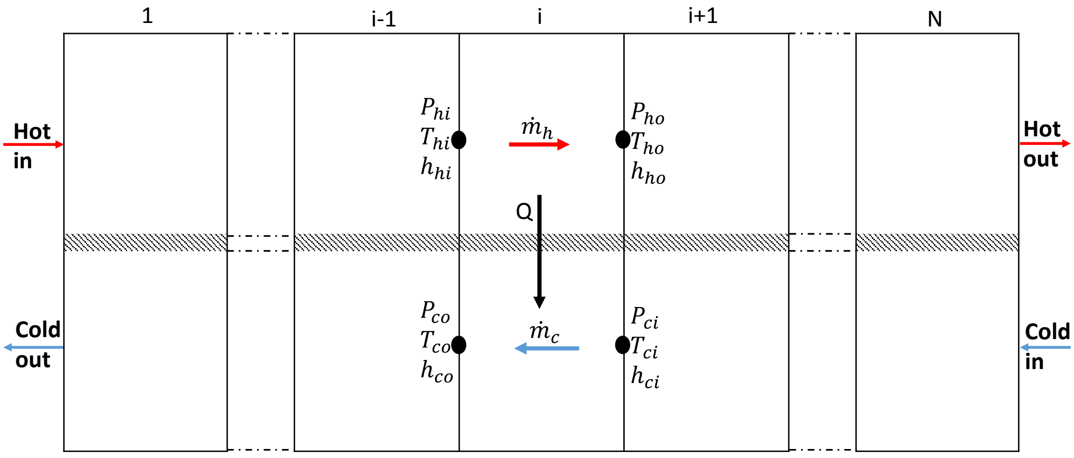

Figure 5 Nodalization of Heat exchanger

For Nitrogen and water, the heat transfer behaviour was estimated by using the Hesselgraves' recommendation for laminar flow and Gnielinski's correlation for turbulent flow as follows[51, 52]:

- Laminar flow (Re<=2300)

$$Nu = 4.089 \tag{24}$$

- Turbulent flow (Re>=5000)

$$Nu = \frac{\frac{f}{8}(Re - 1000)Pr}{1 + 12.7(Pr^{2/3} - 1)\sqrt{\frac{f}{8}}} \tag{25}$$

Where f is the friction factor that can be obtained from the Moody chart or the Colebrook-White correlation:

$$\frac{1}{\sqrt{f}} = -2.0 \log\left(\frac{\varepsilon/D_h}{3.7} + \frac{2.51}{Re\sqrt{f}}\right) \tag{26}$$

- Transition region (2300<Re<5000)

$$Nu = 4.089 + \frac{Nu_{Re=5000} - 4.089}{5000 - 2300}(Re - 2300) \tag{27}$$

For liquid sodium, the Nusselt number was calculated from the Lockart-Martinelli correlation:

$$Nu = 5.0 + 0.025(RePr)^{0.8} \tag{28}$$

Pressure loss, ΔP inside the channel of length L and hydraulic diameter D_h is defined as:

$$\Delta P = f\frac{L}{D_h}\frac{\rho V^2}{2} \tag{29}$$

Where the Darcy friction factor, f for laminar flow is given by:

$$f = \frac{64}{Re} \tag{30}$$

For fully turbulent flow (Re>4000), the Darcy friction factor is given by the Colebrook-White correlation in equation (26).

The heat exchanger thermal-hydraulic design is an iterative process done to achieve the specified effectiveness (or thermal duty) while ensuring that the desired pressure loss was maintained. The total thermal duty is divided equally among the thermal nodes and uniform heat flux is assumed in each node. The calculation can start from either the cold end or the hot end with an initial guess of flow frontal area. Equation (20) to (30) are then applied to determine the fluid conditions, heat transfer coefficients, pressure losses and length of each node. Subsequently, the heat exchanger length and pressure losses on the hot and cold sides are calculated. The calculated pressure loss is compared to the desired pressure loss and if different, a new guess value for the frontal area is selected. The calculation process is repeated until the desired pressure loss is obtained. However, if the calculated length is more than the maximum permissible channel length (2500 mm in this case), a new desired pressure loss is set. Finally, the height, number of module, volume, surface area and mass of the heat exchanger are calculated.

4.2 Turbomachinery design and sizing methodology

The boundary conditions and component parameters selected for the thermodynamic cycles will influence the characteristics and size of the turbomachinery. Hence, preliminary design and sizing was done for the compressors and the turbines in order to highlight the effects of the cycle specifications on the turbomachinery, besides their impact on cycle efficiency. For the nitrogen cycles considered, all the turbomachinery were assumed to be of the axial type due to the large volume flow. Thermodynamic cycle calculation results and specifications such as shaft power or mass flow rate, inlet temperature and pressure, pressure ratio and isentropic efficiency will serve as input design requirements.

The similarity concept is a very common approach for conceptual/preliminary design of turbomachinery [28, 47, 53-56]. It is based on the selection of two dimensionless numbers, specific speed (n_s) and specific diameter (d_s), in conjunction with the use of Balje's n_s-d_s diagrams [57]. n_s and d_s can be determined from equation (31) and equation (32):

$$n_s = \frac{\omega\sqrt{\dot{Q}}}{(gH_{ad})^{3/4}} \quad (31)$$

$$d_s = \frac{D(gH_{ad})^{1/4}}{\sqrt{\dot{Q}}} \quad (32)$$

Where ω is shaft rotational speed, $\dot{Q}$ is the volumetric flow rate, g is acceleration due to gravity, H_{ad} is stage adiabatic head and D is the wheel diameter. From the n_s-d_s diagrams, the values of n_s and d_s needed to achieve the desired turbomachinery efficiency can be determined. Since the volumetric flow rate and total adiabatic head are already fixed by the thermodynamic cycle specifications, the only potential for optimising the turbomachinery design lies with the choice of rotational speed and stage adiabatic head (or number of stages). For the grid connected single shaft configuration, the rotational speed is also fixed and only the number of stages is available for influencing the specific speed. Moreover, there is restriction on the number of stages that can be utilized for turbomachinery design. On the contrary, the two shaft configuration have the advantage to greatly influence the specific speed and hence optimise the efficiency by changing the rotational speed of the compressor shaft.

Even though the similarity concept provides a means to rapidly size the turbomachinery, the n_s-d_s diagrams can only predict approximate value of efficiency. Also, it is only available for single stage compressors and turbines. Therefore, in this study, a more exact but basic and rational preliminary design methodology based on two-dimensional (2-D) mean-line approach was employed. This is because it is not necessary at this initial stage to pursue a detailed design of the turbomachinery. 2-D mean-line analysis means that the flow through the turbomachinery is described by the magnitude and direction of gas velocity in the axial-tangential coordinate at the mean blade height without considering any radial variation in gas flow. Similarly, the thermodynamic properties of the working fluid were specified only at the mean blade height. Thus, fast design solutions can be obtained at the initial phase of turbomachinery design with the 2-D mean-line approach. It is considered a reasonable first approximation for axial-flow turbomachinery with high hub-to-tip ratios greater than 0.8 [58, 59] .

The stator-rotor arrangements for axial-flow turbine and compressor are shown in Figure 6a and Figure 7a respectively. Axial-flow turbine extracts energy from the working fluid by first increasing the tangential velocity of the gas in a row of stator (or nozzle) blades then followed by a row of rotor blades that convert the gas swirl into torque for the rotating shaft. On the other hand, axial-flow compressor compresses the working fluid by first imparting kinetic energy to the fluid by a row of rotor blades then followed by diffusion in a row of stator blades to convert a part of the kinetic energy into static pressure. Several stages are usually needed in axial-flow turbomachinery to attain the required pressure ratio. The relationship among the velocities and flow angles at the inlet and outlet of the rotor is best illustrated with the velocity diagrams at the mean blade height shown in Figure 6b and Figure 7b. The fluid enters the turbine rotor row with a relative velocity, W_2 at an angle, β_2 and leaves with a relative velocity, W_3 at an angle, β_3. The rotor blade tangential velocity at the mean blade height is U. Vectorial addition of the relative velocities and blade velocity yields the absolute velocities C_2 and C_3 at rotor inlet and outlet respectively. For the compressor, the fluid enters the rotor with a relative velocity, W_1 at an angle, β_1 and leaves with a relative velocity, W_2 at an angle, β_2. The corresponding absolute velocities are C_1 and C_2 respectively.

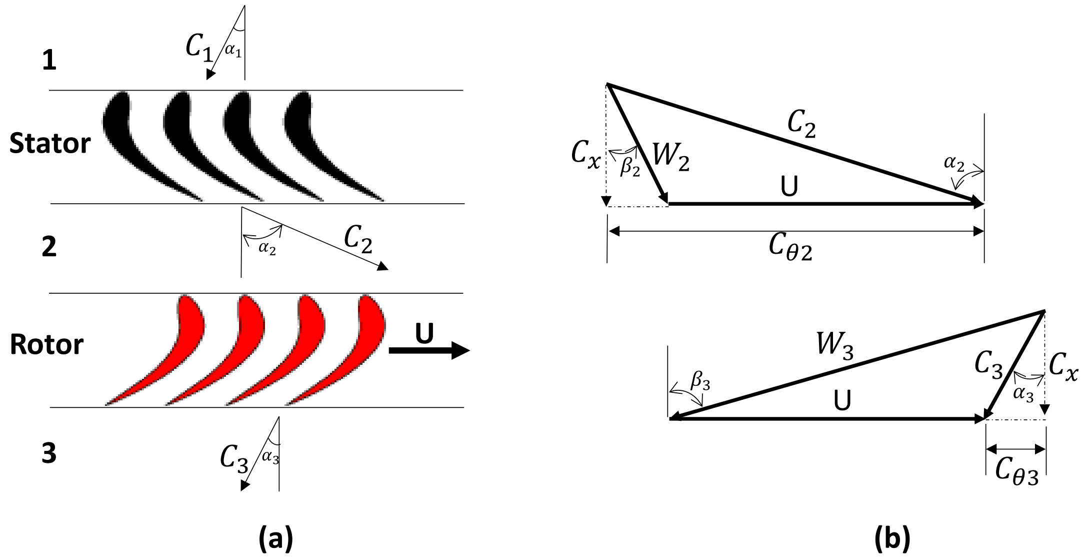

Figure 6 Axial turbine stator-rotor arrangement and velocity diagram

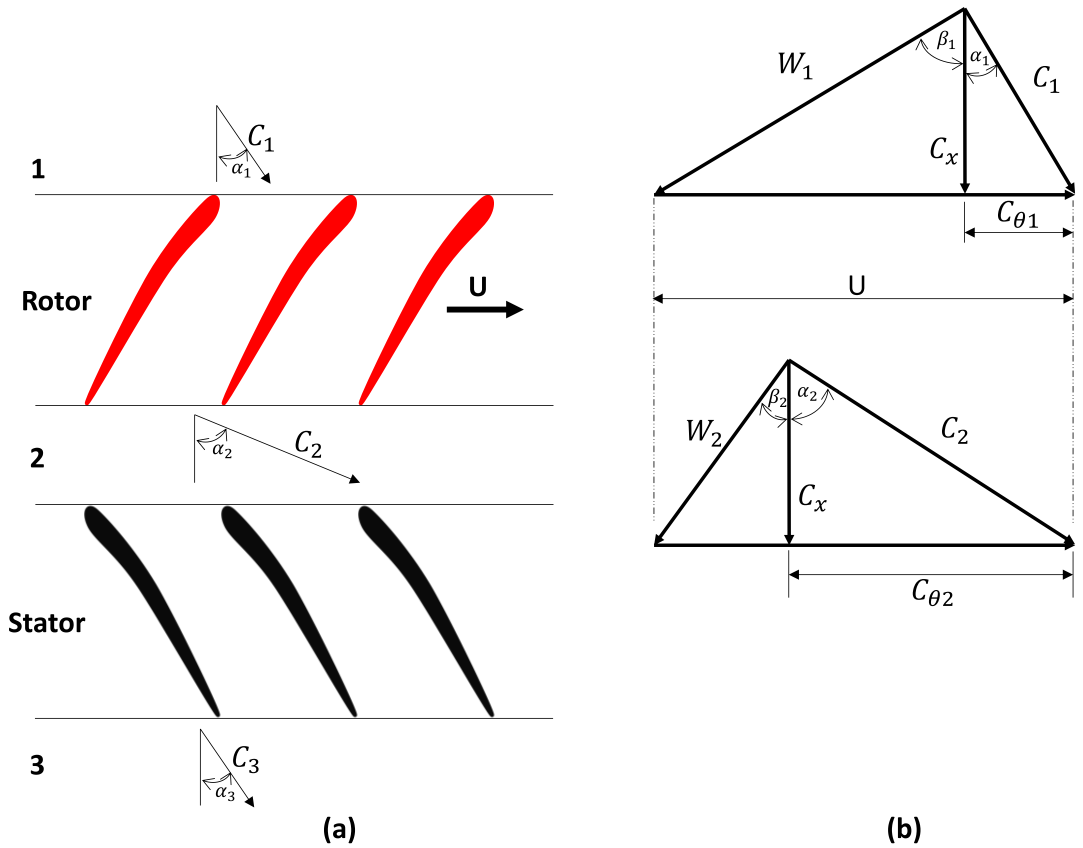

Figure 7Axial compressor rotor-stator arrangement and velocity diagram

Subscript x is used to represent the axial component of the gas velocities while subscript θ represents the tangential components.

Turbomachinery design was performed with the following assumptions:

- The process through the rotor and stator is assumed to be adiabatic

- Constant mean-line blade radius, r_m
- Constant axial-flow velocity, C_x throughout the turbomachinery stages
- Equal enthalpy changes per stage
- Repeating stages used except the first stage of the turbine and final stage of the compressor

Euler turbomachinery equation governing the energy transfer in a turbine stage is given as:

$$\Delta h_0 = U(C_{\theta 2} + C_{\theta 3}) \tag{33}$$

For compressor stage, the Euler equation is given as:

$$\Delta h_0 = U(C_{\theta 2} - C_{\theta 1}) \tag{34}$$

Where,

Δh_0 is the difference in stagnation enthalpy between the stage inlet and exit
$C_{\theta 1}$ is the tangential component of absolute velocity at stage inlet
$C_{\theta 2}$ is the tangential component of absolute velocity at stator exit for turbine or rotor exit for compressor
$C_{\theta 3}$ is the tangential component of absolute velocity at stage exit

The velocity diagrams can be defined by three parameters: flow coefficient, stage loading coefficient and reaction.

The flow coefficient, ϕ is defined as the ratio of axial flow velocity, C_x to the blade velocity, U:

$$\phi = \frac{C_x}{U} \tag{35}$$

The stage loading coefficient, ψ which is a measure of the work done in a stage is defined as:

$$\psi = \frac{\Delta h_0}{U^2} \tag{36}$$

Degree of reaction, Λ shows the fraction of the expansion or compression which occurs in the rotor. It is defined as:

$$\Lambda = \frac{\Delta h_{rotor}}{\Delta h_{stage}} \tag{37}$$

Where,

Δh_{rotor} is the difference in static enthalpy between rotor inlet and exit
Δh_{stage} is the difference in static enthalpy between the stage inlet and exit

Turbine stage performance is specified by total-to-total stage isentropic efficiency and the stator loss coefficient. Turbine stage isentropic efficiency is defined as the ratio of actual work per unit mass to the ideal work per unit mass between the same total pressures:

$$\eta_{T,tt} = \frac{h_{01} - h_{03}}{h_{01} - h_{03,is}} \tag{38}$$

Where,

$\eta_{T,tt}$ is the turbine stage total-to-total isentropic efficiency
h_{01} is the stagnation enthalpy at stage inlet

$h_{\theta 3}$ is the stagnation enthalpy at stage exit
$h_{03,is}$ is the ideal stagnation enthalpy at stage exit with isentropic expansion or compression

The loss coefficient of turbine nozzle blade is determined by the Soderberg's correlation of nominal loss coefficient, ξ:

$$\xi = 0.04 + 0.06\left(\frac{\delta}{100}\right)^2 \tag{39}$$

Where δ is the fluid deflection through the blade.

The loss coefficient is then defined in terms of kinetic energy from the nozzle blade row as [60] :

$$h_2 - h_{2,is} = {}^1\!/_2\, {C_2}^2 \xi \tag{40}$$

Where,
h_2 is the static enthalpy at blade exit
$h_{2,is}$ is the ideal static enthalpy at blade exit with isentropic process
C_2 is the absolute velocity at blade exit

Compressor stage total-to-total efficiency, $\eta_{C,tt}$ is defined as the ratio of the ideal work to the actual work:

$$\eta_{C,tt} = \frac{h_{03,is} - h_{01}}{h_{03} - h_{01}} \tag{41}$$

Since the stage pressure ratios approach unity in this design, the stage efficiency was assumed the same as the polytropic efficiency of the turbomachinery [61] .

The compressor blade loading is assessed by the Liebelin's diffusion factor and de Haller number given in equation (42) and equation (43) respectively:

$$DF = 1 - \frac{V_o}{V_i} + \frac{\Delta V_\theta}{2\sigma V_i} \tag{42}$$

$$dHaller = \frac{V_o}{V_i} \tag{43}$$

Where,
V_i and V_o are the blade inlet and outlet velocity respectively
ΔV_θ is the change in tangential velocity
σ is the blade solidity, which is the ratio of the blade chord to spacing (c/s)

To prevent excessive flow diffusion and potential separation, the diffusion factor should be restricted to below 0.6 and/or the de Haller number should be kept above 0.72. The diffusion factor is used to select the blade solidity which is then used together with the aspect ratio to determine the blade numbers. Aspect ratio, AR is defined the ratio of blade height, b_H to blade chord, c:

$$AR = \frac{b_H}{c} \tag{44}$$

For turbine, Zweifel's criterion for optimum lift coefficient, $C_{L,op}$ is used to determine the solidity as follows:

$$C_{L,op} = \left|\frac{2}{\sigma_x} cos^2 \alpha_o (\tan \alpha_i - \tan \alpha_o)\right| \quad (45)$$

Where,

σ_x is solidity based on axial blade chord

α_i and α_o are the flow angles at blade inlet and outlet respectively

A value of 0.8 is selected for the optimum lift coefficient.

Annulus flow area, A and blade height, b_H can be calculated with the help of mass continuity in equation (46) and equation (47).

$$\dot{m} = \rho A C_x \quad (46)$$

$$A = 2\pi r_m b_H \quad (47)$$

The mean radius, r_m is obtained from:

$$U = r_m \omega \quad (48)$$

The number of blade, N_b is determined from:

$$N_b = \frac{2\pi r_m}{s} \quad (49)$$

Two separate axial-flow turbomachinery design codes were developed in Matlab for the mean-line aerothermodynamic design of the compressors and turbines using the above equations. The design was able to estimate the turbomachinery flowpath geometry, blade heights, gas velocities and flow angles, stage number and volume based on the desired input design requirements obtained from cycle analysis. The main design variables included rotational speed, flow coefficient, stage number, mean blade velocity and inlet flow angle. Thermodynamic properties of the working fluid were obtained from NIST REFPROP property program. Static conditions of the fluid were calculated from the stagnation conditions based on the fundamental principle rather than ideal gas approximation. Similarly, calculations for expansion and compression processes were based on enthalpy instead of the use of constant or average specific heat capacity value. Hence, the codes can be applied to working fluid with real gas properties such as s-CO_2. The turbomachinery design outcome can provide a basis for comparison among different cycles as well as highlighting the impact of various choices of design variables. Also in future work, the preliminary design code can be improved further with the capability for blade profile design, span-line design and generation of performance map for off-design analysis and dynamic modelling.

5 Results and discussion

CBC using nitrogen as working fluid and coupled to SM-SFR was investigated through two cycle configurations: a reference single shaft configuration and a two-shaft configuration with parallel turbines. This section presents the comparison of the two configuration in terms of thermodynamic performance and component design variables.

5.1 Thermodynamic performance

Results of the thermodynamic analysis at the baseline boundary conditions and cycle parameters for each of the two cycle configurations studied is the main output of this section. Hence this will form the basis of thermodynamic performance comparison between the two cycle configuration options.

The Matlab cycle analysis code was used to build a thermodynamic model of the CBCs coupled to SFR using the equations listed in Section 3. A summary of the baseline boundary conditions and parameters used to evaluate the thermodynamic performance of both the reference single-shaft configuration and the proposed two-shaft alternative is shown in Table 5. The boundary conditions (or input variables) include reactor thermal power, reactor outlet temperature and pressure, Na/N_2 IHX primary side outlet temperature, turbine inlet temperature, HPC outlet pressure, LPC inlet pressure, LPC and HPC inlet temperature and cooling water temperature. Typical design parameters such as minimum TTD, heat exchanger and reactor pressure losses, turbomachinery isentropic efficiencies and generator efficiency were used. The input variables and cycle parameters were selected to be the same values for both the single-shaft configuration and the two-shaft alternative. This will ensure a reasonable comparison between the two cycles.

Table 5
Boundary conditions and cycle parameters

Parameter/Variables	**Value**
Reactor thermal power (MW)	500
Core outlet temperature (°C)	545
Core outlet pressure (bar)	1.15
Core pressure loss (bar)	3.74
IHX Na side outlet temperature (°C)	395
Turbine inlet temperature (°C)	530
HPC outlet pressure (bar)	180
LPC and HPC inlet temperatures (°C)	27
Cooling water temperature (°C)	20
Recuperator TTD (°C)	15
Turbomachinery efficiency (%):	
Turbines	93
LP compressor	89
HP compressor	88
Pump	82
Generator efficiency (%)	98.7

As far as possible, heat balance calculation should aim at achieving the maximum cycle efficiency. Only the compressors' pressure ratios are left as variables for optimising the cycle efficiency. Therefore, optimum pressure ratios of the LPC and HPC which make each cycle to reach the maximum thermal efficiencies were determined under the constraints of the specified input variables and cycle parameters. In Figure 8, the cycle efficiency as a function of the LPC inlet pressure and the LPC outlet is plotted. The cycle efficiency shows a maximum value at a LPC inlet pressure of 92.11 bar and a LPC outlet pressure of 125.19 bar (i.e. LPC pressure ratio of 1.36 and HPC pressure of 1.44 after taking into consideration the intercooler pressure loss). The optimum pressure ratios are the same for the two configurations. The Matlab code provides the mass flow rate, pressure, temperature and enthalpy of the working fluid at the inlet and outlet of all the cycle components. Also, the heat transferred and power produced or absorbed in each component were calculated. Then the cycles’ thermal efficiencies were calculated.

Remarkably, the proposed two shaft configuration is able to maintain the thermodynamic performance of the nitrogen cycle in addition to the potential for turbomachinery design optimisation with the free compressor shaft speed. It should be noted that previous studies indicated that two shaft configuration with series turbines usually leads to a deterioration of thermodynamic performance compared to single shaft configuration due to pressure loss in the connecting duct between the HP turbine and the LP turbine [40] . Figure 9 shows the thermodynamic state points of the reference single shaft intercooled configuration for the selected optimum conditions while Figure 10 shows those calculated for the proposed two shaft alternatives. Table 6 presents the major output variables of the thermodynamic performance analysis. The thermodynamic performance results indicated that the two configuration are similar in every respect except that the two shaft configuration employed two parallel turbines with the total flow divided between them.

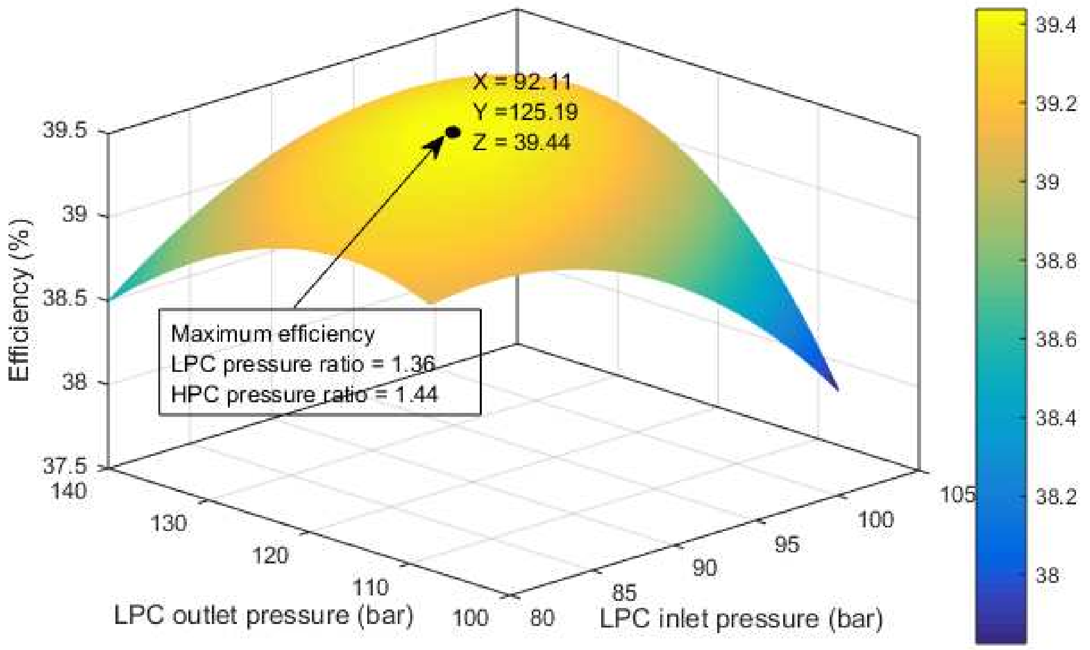

Figure 8 Cycle efficiency as a function of LPC inlet pressure and LPC outlet pressure for both configurations

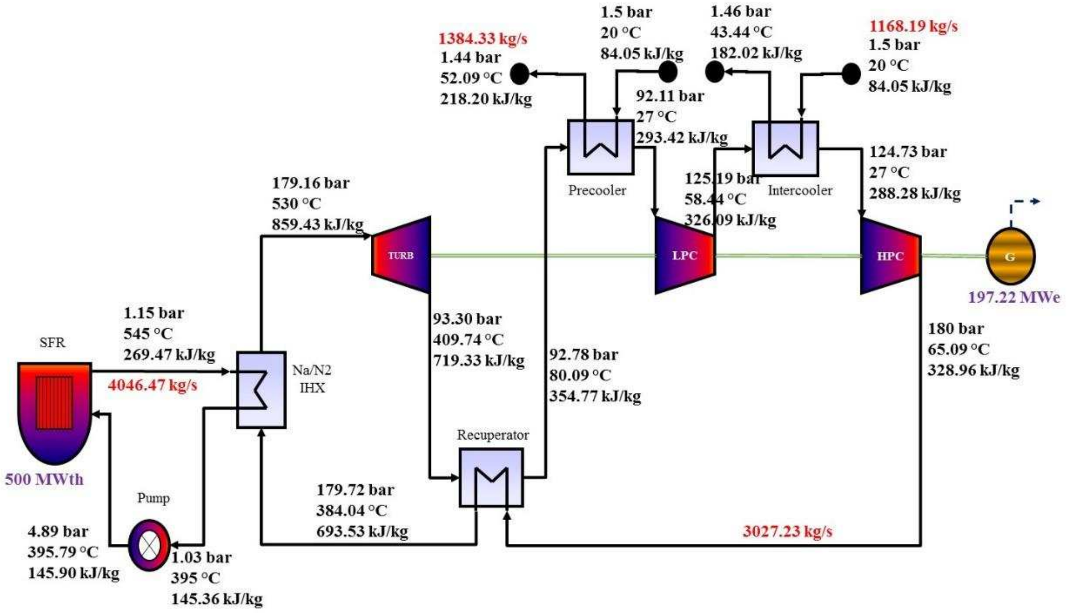

Figure 9 Single shaft configuration thermodynamic state points

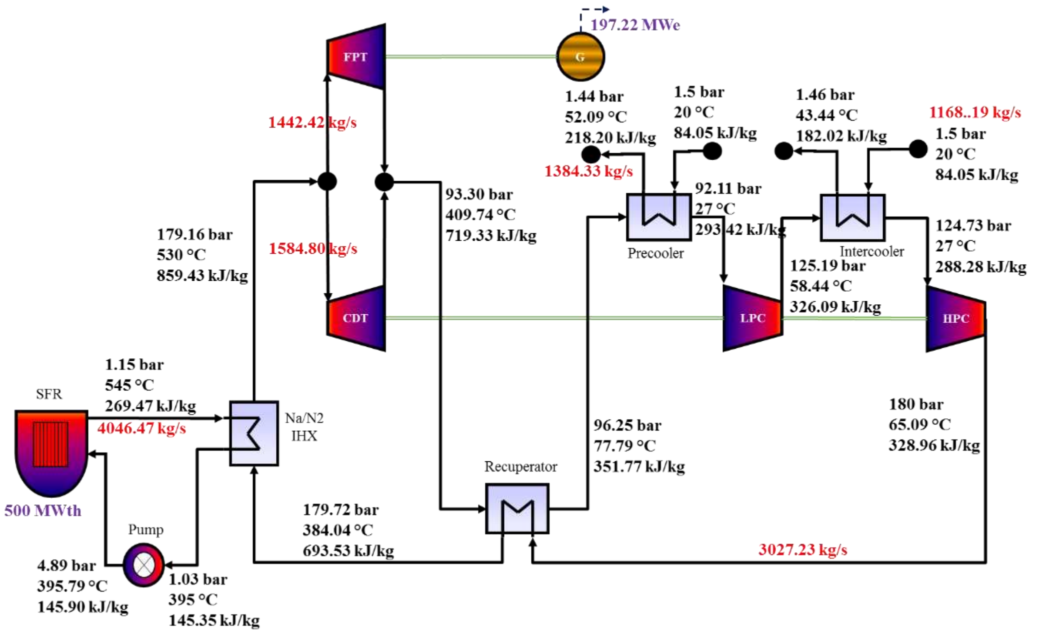

Figure 10 Two shaft configuration thermodynamic state points

Table 6
Thermodynamic performance result

Description	Single shaft	Two shaft
Mass flow rates		
Reactor mass flow	4046.47 kg/s	4046.47 kg/s
FPT	-	1442.42 kg/s
CDT	-	1584.80 kg/s
Total cycle mass flow	3027.23 kg/s	3027.23 kg/s
Precooler cooling water	1384.33 kg/s	1384.33 kg/s
Intercooler cooling water	1168.19 kg/s	1168.19 kg/s
Heat exchanger duty		
Na/N_2 IHX	502.22 MW	502.22 MW
Recuperator	1103.63 MW	1103.63 MW
Precooler	185.70 MW	185.70 MW
Intercooler	114.45 MW	114.45 MW
Heat exchanger effectiveness		
Na/N_2 IHX	94.28 %	94.28 %
Recuperator	95.51 %	95.51 %
Precooler	88.06 %	88.06 %
Intercooler	81.41 %	81.41 %
Turbine power		
CDT	-	222.02 MW
FPT	-	202.07 MW
Total turbine power	424.09 MW	424.09 MW
Compressor power		
LPC	98.88 MW	98.88 MW
HPC	123.14 MW	123.14 MW
Total compressor power	222.02 MW	222.02 MW
Pump load (MW)	2.22 MW	2.22 MW
Pressure ratio (-)		
LPC	1.36	1.36
HPC	1.44	1.44
Turbines	1.92	1.92
Net electrical output	197.22 MWe	197.22 MWe
Cycle efficiency	39.44 %	39.44 %

5.2 Results of heat exchanger design

Heat exchangers of the nitrogen cycle include the Na/N_2 IHX, recuperator, precooler and intercooler. Input design conditions such as the inlet and outlet flow conditions, effectiveness and heat exchanger duties used for the preliminary sizing were obtained from the result of thermodynamic performance analysis given in Figure 9 or Figure 10, and Table 6. Since these values were the same for the single shaft and the two shaft configuration, the heat exchangers design will also be similar. The heat exchangers were discretised into ten thermal nodes. The results of the preliminary design calculations for the heat exchangers are given in Table 7. The temperatures of the heat exchangers' hot and cold streams at the inlet and outlet of the thermal nodes are shown in Figure 11.

The volume of the recuperator alone constitute about 68% of the total volume of the heat exchangers, notwithstanding that the compactness of the recuperator has been improved by using smaller channel diameters, pitch and plate thickness. Any effort to reduce plant size and hence cost should therefore consider the selection and design of the recuperator. The relative large volume of the recuperator is due to the large amount of recuperation and poor heat transfer coefficient between nitrogen gas on both side of the recuperator compared with sodium to nitrogen in the IHX or nitrogen to water in the precooler and intercooler. Also, in this study, conservative design approach was adopted with respect to the channel type, heat conduction length and heat transfer correlation. Thus generally, the sizes of the heat exchangers are likely to be reduced further with a different selection of channel type and a more aggressive design assumption.

The 15 °C baseline minimum TTD chosen for the recuperator seems to be a good compromise between the effect of TTD on recuperator volume and overall cycle efficiency. This is because a slight increase in cycle efficiency by reducing the TTD below 15 °C comes at the cost of very large increase in recuperator volume. The effects of changes in the TTD (or effectiveness) of the recuperator on the overall cycle efficiency and volume of the recuperator are shown in Figure 12. It can be seen that lower TTD causes higher cycle efficiency. A reduction of the recuperator TTD from the baseline value of 15 °C to 5 °C results in a cycle efficiency increase of about 3.3% point. However, the TTD has a significant effect on the volume and hence cost of the recuperator. Decreasing the TTD has a non-linear effect on the recuperator size. The same reduction of TTD from 15 °C to 5 °C results in a recuperator volume increase of about 986% point above the baseline value. On the other hand, an increase in TTD from 15 °C to 25 °C results in about 62% point reduction in recuperator size.

Table 7
Design parameters of heat exchangers

Description	IHX	Recuperator	Precooler	Intercooler
Heat transfer duty (MW)	502.22	1103.63	185.70	114.45
Fluid, hot side/cold side	Na/N_2	N_2/N_2	N_2/Water	N_2/Water
Channel diameter (mm)	2	1.5	2	2
Channel pitch (mm)	2.4	1.9	2.4	2.4
Plate thickness (mm)	1.5	1	1.5	1.5
Number of modules	29	63	23	23
Module width (mm)	900	900	900	900
Module height (mm)	883.56	894.04	885.42	885.05
Module length (mm)	959	2341.9	967.3	878.4
Free flow area (m^2)	5.03	11.79	4	4
Surface area density (m^2/m^3)	714.11	1014.8	714.11	714.11
Thermal density (MW/m^3)	22.70	9.30	10.47	7.11
Hot side pressure loss (kPa)	12	52	67	46
Cold side pressure loss (kPa)	56	28	6	4
Total core volume (m^3)	22.12	118.72	17.73	16.09
Total core mass (kg)	99736	508080	79954	72574

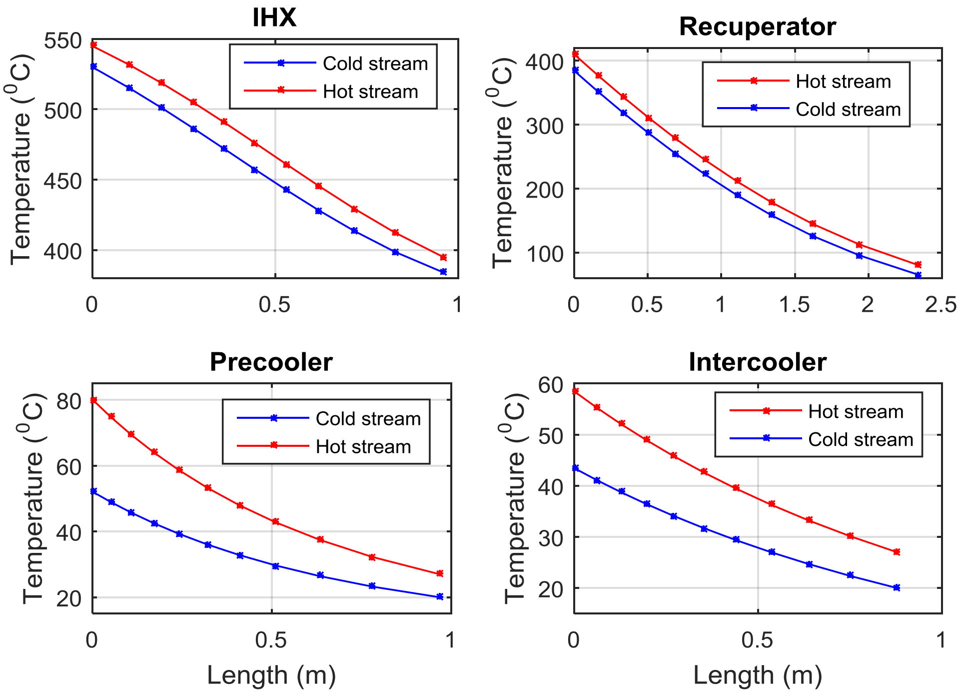

Figure 11 Fluid temperature along heat exchanger length (all counter-current flow)

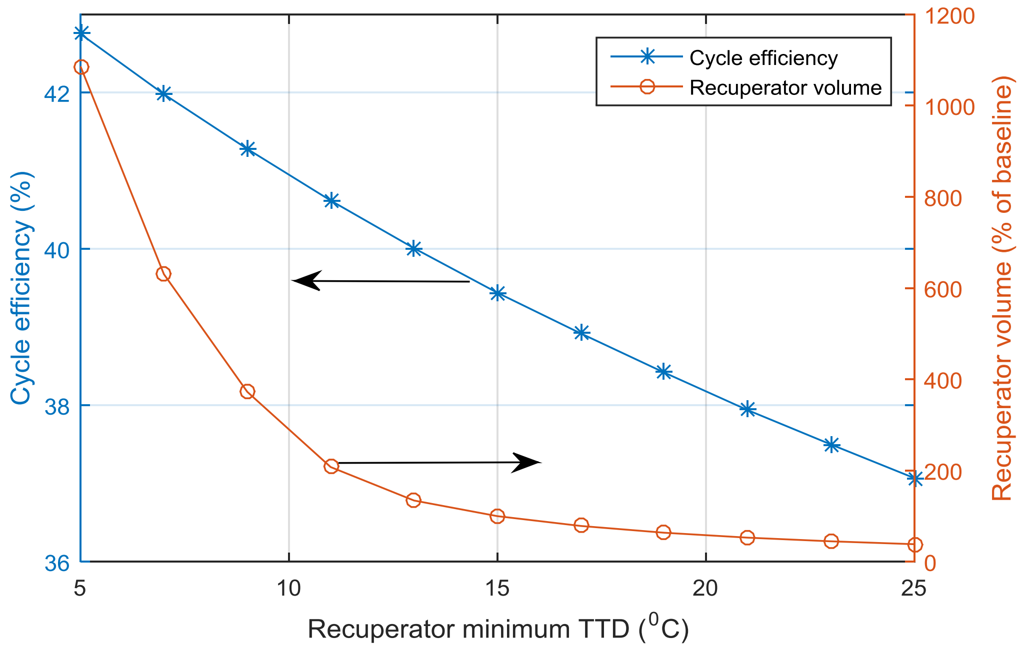

Figure 12 Effects of recuperator TTD on overall cycle efficiency and recuperator volume

5.3 Results of turbomachinery design

In this section, the result of the preliminary design and sizing of the turbomachinery based on 2-D meanline design is presented. The result gives the stage numbers and annular gas flow path geometry of the turbomachinery for the specified input design condition. This provides the basis for assessing the turbomachinery's contribution to the physical size of the plant as well as comparison between the single shaft and the proposed two shaft configuration. Table

8, Table 9 and Table 10 summarise and compare the respective design parameters for the turbines, the LPCs and the HPCs. These tables provide the number of stages, dimensionless design parameters, blade lengths, maximum diameters and other main features for all the turbomachinery.

The approach taken in this work was to design for approximately the same dimensionless parameters of flow coefficient, loading coefficient and reaction for the turbomachinery of the single shaft and two shaft configuration while maintaining the hub-to-tip ratio within acceptable limit. The target flow coefficient, stage loading coefficient and stage reaction for the turbines are about 0.6, 1.1 and 0.5 respectively while the respective values for the compressors are about 0.5, 0.3 and 0.55. The turbine dimensionless parameters were selected to be consistent with operation in the 93% efficiency and 60° nozzle outlet angle region of the ϕ- ψ turbine plot. The ϕ- ψ plot was obtained from Saravanamuttoo et al. [62]. In the case of compressor, no such plot was found. Hence design data from literature was used as a guide in selecting the compressors' dimensionless parameters [63]. Low hub-to-tip ratio will increase secondary losses while too high hub-to-tip ratio will increase the impact of tip clearance losses. Therefore, as much as possible, the hub-to-tip ratio should be kept between 0.75 and 0.90. For the compressors, a de Haller number greater than 0.72 and a diffusion factor lower than 0.4 are sought.

The main reasons for proposing two shaft configuration was to simplify the design of turbomachinery, to reduce turbomachinery size and to provide opportunity for improving cycle efficiency by increasing the efficiency of the turbomachinery.

5.3.1 Turbomachinery design simplification

A shaft speed of 8000 rpm was established as the optimum compressors/CDT rotational speed for the proposed two shaft configuration. The LPC, the HPC and the CDT of the two shaft layout can be freely designed since there is no requirement for a fixed rotational speed. For the reference single shaft configuration, the rotation speed was set to synchronise with the generator speed of 3000 rpm for grid frequency of 50 Hz. Therefore, its turbomachinery all rotate at this speed. Also for the proposed two shaft configuration, the rotational speed of the FPT is fixed at 3000 rpm. The fixing of the generator drive shafts at the synchronous speed will eliminate further losses from the use of gearbox to reduce shaft speed to 3000 rpm or electrical frequency converters to supply electric power at the grid frequency of 50 Hz.

The FPT was designed with one more stage numbers than the stages of the single shaft turbine in order to avoid a hub-to-tip ratio greater than the maximum limit. At a given rotational speed, the number of stages is proportional to the pressure ratio. Thus, the FPT and the single shaft turbine would normally be expected to have the same number of stages since they have the same pressure ratio and rotational speed. However, the hub-to-tip ratio and annular flow area are determined by the flow rate and axial velocity (or blade speed). The FPT's flow rate is lower than the single shaft turbine's flow rate. Therefore, FPT blade speed was reduced to keep the hub-to-tip ratio within acceptable limit while the stage number was increased to bring the loading coefficient to the target value.

5.3.2 Size reduction of the turbomachinery

Design calculation indicated that the total turbine volume is reduced from 3.24 m^3 in the single shaft configuration to 2.2 m^3 in the two shaft configuration due to the reduced tip diameters, although the total number of turbines stages is more for the two-shaft configuration. The size of turbomachinery is a function of both the stage numbers and the tip diameters. For the two shaft CDT, the rotational speed offers extra degree of freedom for design. Hence, the number of stages was reduced to one while appropriate selection of rotational speed was used to maintain the hub-to-tip ratio within the limits. Also, the high rotational speed of the CDT and the reduced blade speed of the FPT lead to reduced tip diameters of the two-shaft configuration turbines compared to the single-shaft turbine.

For the compressors, the total compressors volume is reduced from 1.16 m^3 in the single shaft configuration to 0.2 m^3 in the two shaft configuration. The high rotational speed of the proposed two-shaft configuration resulted in reduced number of compressor stages and reduced tip diameters. In addition, the stage loading coefficient of the two shaft HPC is reduced further in order to keep the hub-to-tip ratio above the minimum limit.

5.3.3 Efficiency improvement

Favourable conditions exist in the proposed two shaft Brayton cycle for improving the turbomachinery efficiencies of the compressors and the CDT. The isentropic efficiencies of the LPC, the HPC and the turbines were assumed in the cycle calculation as 89%, 88% and 93% respectively. These values were also used for the design of the turbomachinery. However, increasing the number of stages and changing the rotational speed are two methods for improving turbomachinery efficiency in a fixed cycle layout [7]. Therefore, the LPC, the HPC and the CDT of the two shaft cycle can be redesigned for a higher efficiency by increasing the number of stages and/or by changing the rotational speed. Better turbomachinery efficiencies will further improve the cycle performance. The effects of isentropic efficiencies of the LPC, the HPC and the CDT on the overall cycle efficiency are shown in Figure 13. The two shaft Brayton cycle shows about 0.29% point rise in cycle efficiency for each 1% point rise in CDT efficiency, about 0.22% point rise in cycle efficiency for each 1% point rise in LPC efficiency, and about 0.27% point rise in cycle efficiency for each 1% rise in HPC efficiency.

Table 8
Turbines design parameters and main features for the nitrogen cycles

Parameters	**Single shaft**	**Two shaft**	
		CDT	**FPT**
Number of stages in turbine	3	1	4
Flow coefficient	0.6	0.6	0.6
Stage loading coefficient	1.08	1.08	1.13
Reaction	0.50	0.50	0.53
Rotational speed, rpm	3000	8000	3000
Maximum tip diameter, mm	1460	926	1210
Maximum tip speed, m/s	229	388	190
Blade height, mm (min/max)	85/135	41/66	56/89
Hub/Tip ratio (min/max)	0.81/0.88	0.86/0.90	0.85/0.90
Blade numbers, (1^{st} stage stator/rotor)	20/76	25/79	26/103
Blade chord, mm (1^{st} stage stator/rotor)	264/284	139/177	173/260
Axial length, mm	2007	304	1785
Volume, m^3	3.24	0.2	2.0
Aspect ratio	3	3	3
Solidity	1.25	1.25	1.25
Pressure ratio (-)	1.92	1.92	1.92
Stage efficiency, %	92.60	93	92.55

Table 9
LPCs design parameters and main features for the nitrogen cycles.

Parameters	Single shaft	Two shaft
Number of stages in LPC	3	1
Flow coefficient	0.5	0.5
Stage loading coefficient	0.29	0.29
Reaction	0.55	0.55
Rotational speed, rpm	3000	8000
Maximum tip diameter, mm	1315	880
Maximum tip speed, m/s	207	369
Blade height, mm (min/max)	67/82	63/79
Hub/Tip ratio (min/max)	0.88/0.90	0.82/0.85
Blade numbers, (1^{st} stage rotor/stator)	64/66	45/50
Blade chord, mm (1^{st} stage rotor/stator)	73/71	68/61
Axial length, mm	440	140
Volume, m^3	0.59	0.08
Aspect ratio	1.1	1.1
Solidity	1.21	1.21
Pressure ratio (-)	1.36	1.36
Stage efficiency, %	89.32	89
de Haller number	0.75	0.75
Diffusion factor	0.39	0.38

Table 10
HPCs design parameters and main features for the nitrogen cycles

Parameters	Single shaft	Two shaft
Number of stages in HPC	4	2
Flow coefficient	0.5	0.5
Stage loading coefficient	0.29	0.25
Reaction	0.55	0.55
Rotational speed, rpm	3000	8000
Maximum tip diameter, mm	1257	760
Maximum tip speed, m/s	197	318
Blade height, mm (min/max)	65/52	62/79
Hub/Tip ratio (min/max)	0.90/0.92	0.79/0.83
Blade numbers, (1^{st} stage rotor/stator)	77/80	37/39
Blade chord, mm (1^{st} stage rotor/stator)	58/48	70/66
Axial length, mm	461	279
Volume, m^3	0.57	0.12
Aspect ratio	1.1	1.1
Solidity	1.21	1.21
Pressure ratio (-)	1.44	1.44
Stage efficiency, %	88.46	88.31
de Haller number	0.75	0.78
Diffusion factor	0.39	0.34

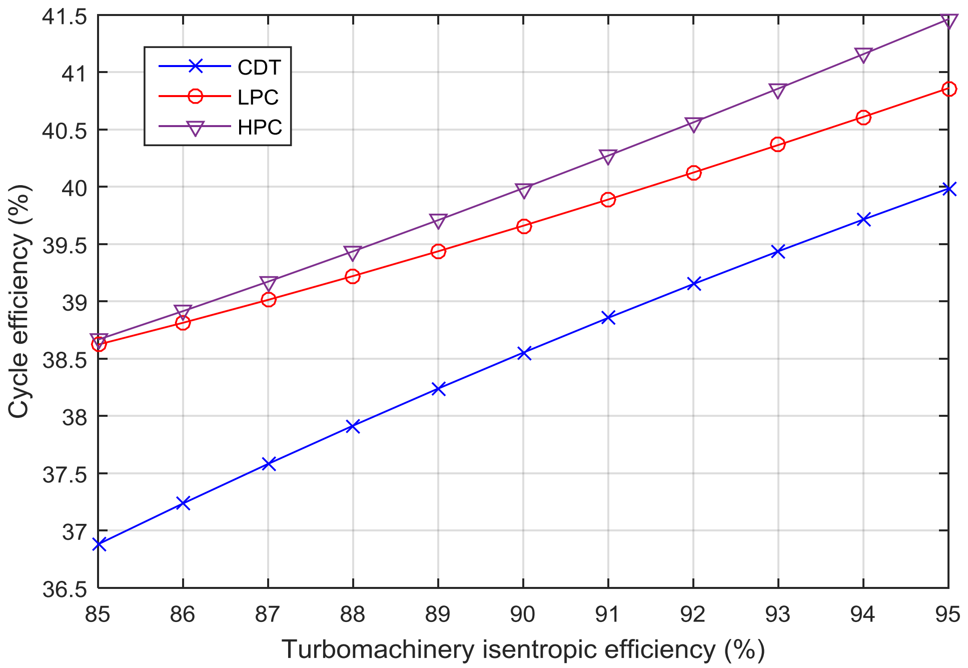

Figure 13 Effect of turbomachinery efficiencies on overall cycle efficiency

6 Conclusions

In this study, thermodynamic analysis and preliminary design of nitrogen CBCs coupled to a 500 MWth SM-SFR have been presented. A reference single-shaft configuration and a proposed two- shaft configuration with parallel turbines were investigated. Thermodynamic performance assessment of the cycles, preliminary sizing of the heat exchangers and 2-D mean-line aerodynamic design of the turbomachinery were performed using models developed in Matlab.

As an outcome of this investigation the following main conclusions can be highlighted:

- Thermodynamic analysis of the cycles indicates that the proposed two shaft configuration with parallel turbines have the same cycle thermodynamic efficiency of 39.44% as the reference single shaft configuration. In contrast, two shaft configuration with turbines in series is known to result in loss of cycle efficiency.
- Heat exchangers preliminary sizing shows that the recuperator constitute a major percentage of the total size. Therefore, any further effort to reduce the plant footprint should focus on the selection and design of the recuperator.
- As expected, cycle efficiency decreases almost linearly with increase in the minimum TTD of the recuperator while recuperator size decreases non-linearly with increase in TTD. Hence, any reduction in volume obtained by increasing the TTD will be at the cost of reduced cycle efficiency. A TTD of 15 ^{0}C appears to be a good compromise between cycle efficiency and recuperator size.
- Preliminary design of the turbomachinery seems to reveal that the proposed two shaft configuration could favour simplification of the design and reduced size as well as increased cycle efficiency by improving the turbomachinery efficiency. The design of the LPC, the HPC and the CDT of the two shaft configuration can be optimised with the shaft rotational speed. An optimum compressors shaft speed of 8000 rpm is established. Total compressors volume is reduced from 1.16 m^3 in the single shaft

configuration to 0.2 m^3 in the two shaft configuration while total turbine volume is reduced from 3.24 m^3 to 2.2 m^3.

In the light of these findings, the proposed two-shaft CBC with nitrogen as working fluid could be a promising PCS for near-term demonstration of electricity generation from SFR. The current preliminary study neglected the impact of the pressure losses in the connecting pipes on the thermodynamic performance. Also the sizing of the heat exchangers is limited to the core, the sizes of the headers are not included. All these can be delayed till the detailed design phase. Nevertheless, this study provides considerable insight into the thermodynamic performance and preliminary sizing of heat exchangers and turbomachinery for nitrogen CBC coupled to SM-SFR.

Future studies should investigate opportunities for improving the heat transfer performance of the recuperator and hence reduction in recuperator size by (1) using wavy channel instead of straight channel type (2) assuming a shorter heat conduction length and (3) using a more radical heat transfer relationship obtained from experimental validation. On the other hand, more compact heat exchanger type such as the plate fin heat exchanger [64] should be investigated as substitute for the PCHE. However, this could be at the expense of the reduced risk of development offered by PCHE.

Acknowledgement

The authors would like to acknowledge GE Power (formerly ALSTOM Power Ltd) for financial support of this research.

References

[1] L. Damiani, A. P. Prato, and R. Revetria, "Innovative steam generation system for the secondary loop of “ALFRED” lead-cooled fast reactor demonstrator," Applied Energy, vol. 121, pp. 207-218, 2014.

[2] F. Carre, P. Yvon, P. Anzieu, N. Chauvin, and J.-Y. Malo, "Update of the French R&D strategy on gas-cooled reactors," Nuclear Engineering and Design, vol. 240, no. 10, pp. 2401-2408, 2010.

[3] G. D. Pérez-Pichel, J. I. Linares, L. E. Herranz, and B. Y. Moratilla, "Thermal analysis of supercritical CO2 power cycles: Assessment of their suitability to the forthcoming sodium fast reactors," Nuclear Engineering and Design, vol. 250, pp. 23-34, 2012.

[4] B. Merk, A. Stanculescu, P. Chellapandi, and R. Hill, "Progress in reliability of fast reactor operation and new trends to increased inherent safety," Applied Energy, vol. 147, pp. 104-116, 2015.

[5] Gen IV International Forum (GIF), "Technology roadmap update for Generation IV nuclear energy systems," Nuclear Energy Agency (NEA) of the Organisation for Economic Co-operation and Development (OECD), Paris, 2014, Available: https://www.gen-4.org/gif/upload/docs/application/pdf/2014-03/gif-tru2014.pdf, Accessed on: 6 May 2015.

[6] P. G. Rousseau and J. P. Van Ravenswaay, "Thermal-fluid comparison of three-and single-shaft closed loop brayton cycle configurations for HTGR power conversion," in Proceedings of international congress on advances in nuclear power plants *(ICAPP’03)*, Cordoba, Spain, 2003.

[7] Y. Ahn and J. I. Lee, "Study of various Brayton cycle designs for small modular sodium-cooled fast reactor," Nuclear Engineering and Design, vol. 276, pp. 128-141, 2014.

[8] S. Hong, C. J. A. Bradshaw, and B. W. Brook, "Global zero-carbon energy pathways using viable mixes of nuclear and renewables," Applied Energy, vol. 143, pp. 451-459, 2015.
[9] P. Eser, A. Singh, N. Chokani, and R. S. Abhari, "Effect of increased renewables generation on operation of thermal power plants," Applied Energy, vol. 164, pp. 723-732, 2016.
[10] A. S. Brouwer, M. van den Broek, W. Zappa, W. C. Turkenburg, and A. Faaij, "Least-cost options for integrating intermittent renewables in low-carbon power systems," Applied Energy, vol. 161, pp. 48-74, 2016.
[11] V. Krakowski, E. Assoumou, V. Mazauric, and N. Maïzi, "Reprint of Feasible path toward 40–100% renewable energy shares for power supply in France by 2050: A prospective analysis," Applied Energy, vol. 184, pp. 1529-1550, 2016.
[12] G. D. Pérez-Pichel, J. I. Linares, L. E. Herranz, and B. Y. Moratilla, "Potential application of Rankine and He-Brayton cycles to sodium fast reactors," Nuclear Engineering and Design, vol. 241, no. 8, pp. 2643-2652, 2011.
[13] S. B. Seo, H. Seo, and I. C. Bang, "Adoption of nitrogen power conversion system for small scale ultra-long cycle fast reactor eliminating intermediate sodium loop," Annals of Nuclear Energy, vol. 87, Part 2, pp. 621-629, 2016.
[14] O. Olumayegun, M. Wang, and G. Kelsall, "Closed-cycle gas turbine for power generation: A state-of-the-art review," Fuel, vol. 180, pp. 694-717, 2016.
[15] J. R. Hoffmann and E. G. Feher, "150 kwe supercritical closed cycle system," Journal of Engineering for Gas Turbines and Power, vol. 93, no. 1, pp. 70-80, 1971.
[16] Y. Ahn et al., "Review of supercritical CO2 power cycle technology and current status of research and development," Nuclear Engineering and Technology, vol. 47, no. 6, pp. 647-661, 2015.
[17] V. Dostal, "A supercritical carbon dioxide cycle for next generation nuclear reactors," PhD Thesis, Massachusetts Institute of Technology (MIT), Cambridge, Massachusetts, USA, 2004.
[18] L. Santini, C. Accornero, and A. Cioncolini, "On the adoption of carbon dioxide thermodynamic cycles for nuclear power conversion: A case study applied to Mochovce 3 Nuclear Power Plant," Applied Energy, vol. 181, pp. 446-463, 2016.
[19] X. Wang and Y. Dai, "Exergoeconomic analysis of utilizing the transcritical CO2 cycle and the ORC for a recompression supercritical CO2 cycle waste heat recovery: A comparative study," Applied Energy, vol. 170, pp. 193-207, 2016.
[20] R. V. Padilla, Y. C. Soo Too, R. Benito, and W. Stein, "Exergetic analysis of supercritical CO2 Brayton cycles integrated with solar central receivers," Applied Energy, vol. 148, pp. 348-365, 2015.
[21] R. V. Padilla, Y. C. S. Too, R. Benito, R. McNaughton, and W. Stein, "Thermodynamic feasibility of alternative supercritical CO2 Brayton cycles integrated with an ejector," Applied Energy, vol. 169, pp. 49-62, 2016.
[22] B. D. Iverson, T. M. Conboy, J. J. Pasch, and A. M. Kruizenga, "Supercritical CO2 Brayton cycles for solar-thermal energy," Applied Energy, vol. 111, no. 0, pp. 957-970, 2013.
[23] S. J. Bae, Y. Ahn, J. Lee, and J. I. Lee, "Various supercritical carbon dioxide cycle layouts study for molten carbonate fuel cell application," Journal of Power Sources, vol. 270, pp. 608-618, 2014.
[24] M. Mecheri and Y. Le Moullec, "Supercritical CO2 Brayton cycles for coal-fired power plants," Energy, vol. 103, pp. 758-771, 2016.
[25] S. Banik, S. Ray, and S. De, "Thermodynamic modelling of a recompression CO2 power cycle for low temperature waste heat recovery," Applied Thermal Engineering, vol. 107, pp. 441-452, 2016.

[26] H. S. Pham et al., "Mapping of the thermodynamic performance of the supercritical CO2 cycle and optimisation for a small modular reactor and a sodium-cooled fast reactor," Energy, vol. 87, pp. 412-424, 2015.
[27] W. S. Jeong, J. I. Lee, and Y. H. Jeong, "Potential improvements of supercritical recompression CO2 Brayton cycle by mixing other gases for power conversion system of a SFR," Nuclear Engineering and Design, vol. 241, no. 6, pp. 2128-2137, 2011.
[28] J.-E. Cha et al., "Development of a supercritical CO2 Brayton energy conversion system coupled with a sodium cooled fast reactor," Nuclear Engineering and Technology, vol. 41, no. 8, pp. 1025-1044, 2009.
[29] J. J. Sienicki et al., "International collaboration on development of the supercritical carbon dioxide Brayton cycle for Sodium-cooled Fast Reactors under the Generation IV International Forum Component Design and Balance of Plant project," in Proceedings of the 2010 International Congress on Advances in Nuclear Power *Plants (ICAPP'10)*, San Diego, USA, pp. 392-399.
[30] A. Moisseytsev and J. J. Sienicki, "Investigation of alternative layouts for the supercritical carbon dioxide Brayton cycle for a sodium-cooled fast reactor," Nuclear Engineering and Design, vol. 239, no. 7, pp. 1362-1371, 2009.
[31] J. J. Sienicki, A. Moisseytsev, and L. Krajtl, "A Supercritical CO2 Brayton Cycle Power Converter for a Sodium-Cooled Fast Reactor Small Modular Reactor," in ASME 2015 Nuclear Forum collocated with the ASME 2015 Power Conference, the ASME 2015 9th International Conference on Energy Sustainability, and the ASME 2015 13th International Conference on Fuel Cell Science, Engineering and Technology, 2015: American Society of Mechanical Engineers.
[32] A. Dragunov, E. Saltanov, S. Bedenko, and I. Pioro, "A Feasibility Study on Various Power-Conversion Cycles for a Sodium-Cooled Fast Reactor," in 2012 20th International Conference on Nuclear Engineering and the ASME 2012 Power Conference, 2012, pp. 559-567: American Society of Mechanical Engineers.
[33] J.-H. Eoh, H. C. No, Y.-B. Lee, and S.-O. Kim, "Potential sodium–CO2 interaction of a supercritical CO2 power conversion option coupled with an SFR: Basic nature and design issues," Nuclear Engineering and Design, vol. 259, pp. 88-101, 2013.
[34] Y. Sun, Y. Zhang, and Y. Xu, "Study on coupling a gas turbine cycle to HTR-10 test reactor," in Proceedings of Technical Committee Meeting on Gas Turbine Power Conversion Systems for Modular HTGRs, Palo Alto, California (United States), 2000, vol. IAEA-TECDOC-1238, pp. 42-51, Vienna, Austria: International Atomic Energy Agency (IAEA), 2001.
[35] N. Alpy et al., "Gas cycle testing opportunity with ASTRID, the French SFR prototype," in Proceedings of Supercritical CO2 Power Cycle Symposium, Boulder, Colorado (USA), 2011.
[36] M. Saez, D. Haubensack, N. Alpy, A. Gerber, and F. Daid, "The use of gas based energy conversion cycles for sodium fast reactors," in Proceedings of the 2008 International Congress on Advances in Nuclear Power Plants-ICAPP'08, Anaheim, CA, 2008, Illinois, USA: American Nuclear Society, 555 North Kensington Avenue, La Grange Park, 2008.
[37] L. Cachon et al., "Innovative power conversion system for the French SFR prototype, ASTRID," in Proceedings of the 2012 International Congress on Advances in Nuclear Power Plants - ICAPP '12, Chicago,IL, 2012, Illinois, USA: American Nuclear Society, 555 North Kensington Avenue, La Grange Park, 2012.
[38] French Alternative Energies and Atomic Energy Commission (CEA), "4th-Generation sodium-cooled fast reactor: The ASTRID technological demonstrator," CEA Nuclear Energy Division., Paris, 2012, Available: http://www.cea.fr/multimedia/Documents/publications/rapports/rapport-gestion-durable-matieres-nucleaires/4th-generation-sodium-cooled-fast-reactors.pdf, Accessed on: 10 November 2015.

[39] P. P. Walsh and P. Fletcher, Gas turbine performance, 2nd ed. Oxford: John Wiley and Sons, 2004.

[40] J. Lee, J. I. Lee, Y. Ahn, and M. Choi, "Preliminary study of helium Brayton cycle turbomachinery for small modular high temperature gas cooled reactor application," in Proceedings of the 2013 International Congress on Advances in Nuclear Power *Plants (ICAPP'13)*, Jeju Island, Korea, 2013: Korea Nuclear Society.

[41] V. Sobolev, "Database of thermophysical properties of liquid metal coolants for GEN-IV," Belgian Nuclear Research Centre (SCK.CEN), Mol, Belgium, 2011, Available: http://hdl.handle.net/10038/7739, Accessed on: 08 April 2015.

[42] E. W. Lemmon, M. L. Huber, and M. O. McLinden, "NIST Standard Reference Database 23: Reference Fluid Thermodynamic and Transport Properties-REFPROP," Version 9.1 ed. Gaithersburg: National Institute of Standards and Technology (NIST), 2013.

[43] N. A. Carstens, "Control Strategies for Supercritical Carbon Dioxide Power Conversion Systems," PhD Thesis, Massachusetts Institute of Technology (MIT), Cambridge, Massachusetts, USA, 2007.

[44] J. Floyd et al., "A numerical investigation of the sCO2 recompression cycle off-design behaviour, coupled to a sodium cooled fast reactor, for seasonal variation in the heat sink temperature," Nuclear Engineering and Design, vol. 260, no. 0, pp. 78-92, 2013.

[45] J. C. Bryant, H. Saari, and K. Zanganeh, "An analysis and comparison of the simple and recompression supercritical CO2 cycles," in Proceedings of Supercritical CO2 Power Cycle Symposium, Boulder, Colorado (USA), 2011.

[46] P. M. Fourspring and J. P. Nehrbauer, "Heat exchanger testing for closed Brayton cycle using supercritical CO2 as working fluid," in Proceedings of Supercritical CO2 Power Cycle Symposium, Boulder, Colorado (USA), 2011.

[47] S. A. Wright, M. E. Vernon, and P. S. Pickard, "Concept Design for a High Temperature Helium Brayton Cycle with Interstage Heating and Cooling," Sandia National Laboratories (SNL), Albuquerque, New Mexico and Livermore, California, 2006, Available: http://nuclear.inel.gov/deliverables/docs/genivihc_2006_milestone_report_7_1_2006_final.pdf.

[48] R. K. Shah and D. P. Sekulic, Fundamentals of heat exchanger design. New Jersey: John Wiley and Sons, 2003.

[49] R. Le Pierres, D. Southall, and S. Osborne, "Impact of mechanical design issues on printed circuit heat exchangers," in Proceedings of Supercritical CO2 Power Cycle Symposium, Boulder, Colorado (USA), 2011.

[50] Q. Li, G. Flamant, X. Yuan, P. Neveu, and L. Luo, "Compact heat exchangers: A review and future applications for a new generation of high temperature solar receivers," Renewable and Sustainable Energy Reviews, vol. 15, no. 9, pp. 4855-4875, 2011.

[51] J. E. Hesselgreaves, Compact heat exchangers: selection, design and operation. Oxford (UK): Elsevier Science Ltd, 2001.

[52] V. Dostal, M. J. Driscoll, and P. Hejzlar, "A supercritical carbon dioxide cycle for next generation nuclear reactors," The MIT Centre for Advanced Nuclear Energy Systems, Cambridge, Massachusetts (USA), MIT-ANP-TR-100, 2004, Available: http://web.mit.edu/22.33/www/dostal.pdf.

[53] S. J. Bae, J. Lee, Y. Ahn, and J. I. Lee, "Preliminary studies of compact Brayton cycle performance for Small Modular High Temperature Gas-cooled Reactor system," Annals of Nuclear Energy, vol. 75, no. 0, pp. 11-19, 2015.

[54] J. J. Sienicki, A. Moisseytsev, R. L. Fuller, S. A. Wright, and P. S. Pickard, "Scale dependencies of supercritical carbon dioxide Brayton cycle technologies and the optimal size for next-step supercritical CO2 cycle demonstration," in Proceedings of Supercritical CO2 Power Cycle Symposium, Boulder, Colorado (USA), 2011.

[55] Y. Gong, N. A. Carstens, M. J. Driscoll, and I. A. Matthews, "Analysis of Radial Compressor Options for Supercritical CO2 Power Conversion Cycles," Center for Advanced Nuclear Energy Systems, MIT Department of Nuclear Science and Engineering, and MIT Gas Turbine Laboratory of the Department of Aeronautics and Astronautics., Cambridge, Massachussetts (USA), MIT-GFR-034, 2006, Available: http://nuclear.inl.gov/deliverables/docs/topical_report_mit-gfr-034.pdf, Accessed on: 09 March 2014.

[56] R. L. Fuller and W. Batton, "Practical considerations in scaling supercritical carbon dioxide closed Brayton cycle power systems," in Proceedings of Supercritical CO2 Power Cycle Symposium, Troy, New York (USA), 2009.

[57] O. Balje, Turbomachines. A guide to Design, Selection and Theory. New York: John Wiley and Sons, 1981.

[58] W. W. Bathie, Fundamentals of gas turbines, 2nd ed. New York: John Wiley and Sons, 1996.

[59] R. S. R. Gorla and A. A. Khan, Turbomachinery: design and theory. New York: Marcel Dekker Inc, 2003.

[60] S. L. Dixon, Fluid mechanics, thermodynamics of turbomachinery, 5th ed. Oxford: Elsevier Inc, 1998.

[61] J. D. Mattingly, Elements of gas turbine propulsion: Gas turbines and rockets. Reston, VA: American Institute of Aeronautics and Astronautics (AIAA), 2006.

[62] H. I. H. Saravanamuttoo, G. F. C. Rogers, H. Cohen, and P. Straznicky, Gas Turbine Theory, 6th ed. Essex (UK): Prentice Hall, Pearson Education, 2009.

[63] J. Wang and Y. Gu, "Parametric studies on different gas turbine cycles for a high temperature gas-cooled reactor," Nuclear Engineering and Design, vol. 235, no. 16, pp. 1761-1772, 2005.

[64] C. Wang, Balance of Plant Analysis for High Temperature Gas Cooled Reactors: Design and Optimization of Gas Turbine Power Conversion System, and Component Design of Turbo-Machinery for Modular Pebble Bed Reactor Plants. Saarbrücken (Germany): Lambert Academic Publishing, 2009.